

Article

Application of Model-Free and Model-Based Kinetic Methods in Evaluation of Reactions Complexity during Thermo-Oxidative Degradation Process: Case Study of [4-(Hydroxymethyl)phenoxyethyl] Polystyrene Resin

Bojan Janković ^{1,*}, Vladimir Dodevski ¹, Filip Veljković ¹, Marija Janković ¹ and Nebojša Manić ²

¹ “Vinča” Institute of Nuclear Sciences—National Institute of the Republic of Serbia, University of Belgrade, Mike Petrovića Alasa 12-14, 11001 Belgrade, Serbia; vladimir@vinca.rs (V.D.); filipveljkovic@vinca.rs (F.V.); marijam@vinca.rs (M.J.)

² Laboratory for Thermal Analysis, Faculty of Mechanical Engineering, University of Belgrade, Kraljice Marije 16, 11120 Belgrade, Serbia; nmanic@mas.bg.ac.rs

* Correspondence: bojan.jankovic@vinca.rs

Abstract: This work examined the possibilities and limitations of model-free and model-based methods related to decrypting the kinetic complexity of multi-step thermo-oxidative degradation processes (as a testing system, a [4-(hydroxymethyl)phenoxyethyl] polystyrene resin was used), monitored by thermal analysis (TGA-DTG-DTA) techniques. It was found that isoconversional methods could successfully determine the correct number of process stages and presence of multiple reactions based on derived $E_a(\alpha)$ profiles and identify the negative dependence of the rate constant on the temperature. These methods could not overcome the problem that arose due to mass transfer limitations. The model-based method overcame more successfully the problem associated with mass transfer because its calculation machinery had capabilities for the correct solution of the total mass balance equation. However, a perfect fit with the experimental data was not achieved due to the dependence on the thermal history of the contribution ($ctb.$) of a given reaction step inside a fitting procedure cycle. On the other hand, through this approach, it was possible to estimate the rate-controlling steps of the process regarding the influence of the heating rate. It was found that for consecutive reaction mechanisms, the production of benzaldehyde and gases in high yields was controlled by the heating rate, where low heating rates were strongly recommended ($\leq 10 \text{ K/min}$). Also, it was shown that the transport phenomenon may be also the rate-determining step (within the set of “intrinsic” kinetic parameters). It was also established that external heat transfer controls the overall rate, where the “pure” kinetic control regime had not been reached but was approached when lowering the temperature and size of the resin particles.

Keywords: isoconversional approach; model-based calculations; multiple-step process; mass and heat transfers; autocatalysis; exothermicity



Citation: Janković, B.; Dodevski, V.; Veljković, F.; Janković, M.; Manić, N. Application of Model-Free and Model-Based Kinetic Methods in Evaluation of Reactions Complexity during Thermo-Oxidative Degradation Process: Case Study of [4-(Hydroxymethyl)phenoxyethyl] Polystyrene Resin. *Fire* **2024**, *7*, 165. <https://doi.org/10.3390/fire7050165>

Academic Editor: Ali Cemal Benim

Received: 27 March 2024

Revised: 2 May 2024

Accepted: 9 May 2024

Published: 11 May 2024



Copyright: © 2024 by the authors. Licensee MDPI, Basel, Switzerland. This article is an open access article distributed under the terms and conditions of the Creative Commons Attribution (CC BY) license (<https://creativecommons.org/licenses/by/4.0/>).

1. Introduction

Due to the often complex nature of solid-state kinetics and issues associated with separating effects of the temperature-dependent rate constant ($k(T)$) and conversion function ($f(\alpha)$), principally, isoconversional methods (wherein the conversion is fixed) have withstood the “pessimistic view” [1] towards non-isothermal kinetic data analysis. Isoconversional methods can be used to define the dependence of the apparent activation energy (E_a) on the conversion (α) ($E_a = E_a(\alpha)$) to help the interpret reaction complexities during thermally induced process if they exist, rather than relegate them to a mere inconvenience, for methods that assume a single-step reaction [2]. So, the nature of the Arrhenius equation dictates that the activation energy is the principal result from the isoconversional analysis [3]. By applying the isoconversional principle, it is possible to eliminate the reaction

model from the calculation related to the rate of thermally stimulated processes. This principle states that the rate of process at the constant degree of conversion is a function of temperature only. Therefore, it follows that the activation energy can be established from the temperature dependence of the conversion rate of the process (the temperature dependence of the (iso)conversion rate can be obtained by a series of measurements at different temperature programs, i.e., heating rates, β , without previously determining the reaction model. This is the reason why isoconversional methods are called model-free methods (this expression should not be taken literally because although these methods do not imply the determination of a reaction model, they assume that the dependence of the degree of conversion on the rate of process is in accordance with some of the known forms of mathematical functions of reaction models, which are proposed in the literature). However, it must be noted that the validity of all isoconversional methods is critically dependent on the isoconversional principle, i.e., the theory that the conversion rate is a function only of temperature at a set of conversion values [4]. This principle is only guaranteed to hold if an entire conversion range is built up from non-overlapped steps, but this would indicate the multi-step character of the process [2].

It has been convincingly demonstrated that the best pathway to identify any form of complex kinetics is to perform an isoconversional analysis, which was shown in earlier works that dealt with this issue [1,5]. However, the application of the isoconversional kinetic approach can be very difficult if the task is to differentiate between a number of reactions with very similar activation energies [6] or in the case where the isoconversional principle is no longer valid. Because of the difficulty in modeling any type of process complexity, there was a need to give some general instructions regarding the collection of experimental thermal analysis data for the kinetic computation's implementation [7], then provide general recommendations for the kinetic analysis of thermal degradation, investigated by thermal analysis techniques and focusing on the specific classes of materials (inorganic, organic and polymeric materials, as well as biomass and solid fuels, respectively) [8], and finally, give recommendations for the analysis of multi-step kinetics [9]. All these recommendations were presented by the International Confederation for Thermal Analysis and Calorimetry (ICTAC) [9]. Current recommendations strongly suggest the mandatory use of model-free kinetic methods as well as mathematical fit, without understanding the mechanisms of the process behind it: the application without queries! The dependence of the apparent activation energy determined by model-free methods makes it possible to carry out a significant analysis of the "level of kinetic complexity" of an examined process. Due to complicated physicochemical processes, E_a may vary as a function of reaction progress.

Additionally, a worthy "rival" to isoconversional (model-free) kinetic methods, model-fitting (or model-based) kinetic methods are often used in the kinetic consideration of processes and refer to the practice of assuming the mathematical form of a kinetic model and approximating its kinetic parameters (the activation energy and pre-exponential factor) based on that assumption. Specifying the correct function of conversion is absolutely critical and allows both the activation energy and pre-exponential factor to be determined simultaneously. If this method is applied to insufficient data or a low standard of correlation is accepted, then the erroneous mechanism selection, which is almost certain to occur, will lead to meaningless kinetic parameters. Today, with the development of modern computation software, many problems can be overcome because the approach associated with model-based analysis includes the determination of the kinetic triplet [E , A , and $f(\alpha)$] through the application of the multivariate non-linear regression (MVNLR) procedure [10]. Modern software packages include operating tool systems with a detailed statistical evaluation of generated kinetic quantities based on their quality of fits to corresponding experimental thermo-analytical signals for both isothermal and non-isothermal tests of various processes.

The aim of this work is to examine the possibilities as well as limitations of model-free and model-based methods in the determination of the kinetic parameters of the complex

thermo-oxidative process. The results from the model-free analysis were compared with the results of the model-based analysis in order to test the reliability of the used methods in determining the kinetic parameters and for the identification of the types of kinetic models, which govern the entire thermo-oxidative process. Three model-free methods were used in this work, the Friedman (FR) method [11], the Vyazovkin (VY) advanced method [12] (pp. 1–59), and the numerical (NM) (optimization) method [9], respectively. These methods were used in providing the proper search range for the model-based analysis, which operated with MVNLR. All kinetic calculations were carried out on the basis of collected simultaneous thermo-analytical measurements at four different heating rates in an air atmosphere, using thermogravimetry (TG), derivative thermogravimetry (DTG), and differential thermal analysis (DTA) techniques.

In this study, the oxidative characteristics and kinetics of a high-purity ion-exchange resin—[4-(hydroxymethyl)phenoxyethyl] polystyrene resin (Supplementary Material—Section S.I.; Table S1) were investigated. It should be noted that ion-exchange resins, mostly polystyrenic resins, are widely used for water treatment in nuclear power plants because of their ability to remove impurities from cooling water coils. Embedded “spent” resins can undergo radiolytic or chemical degradation, which may result in the emission of hazardous species into the environment. So, combustion and pyrolysis could be used as decomposition techniques with the objective of reducing the waste volume and making the final waste more chemically stable. On the other hand, thermo-chemical technologies can have great potential for recycling polystyrene-based materials into new materials or value-added products. In this context, the combustion process may provide a sustainable pathway for polystyrene (PS)-based resins’ conversion to value-added products. Given the structure and chemical properties of the resin under investigation here (Supplementary Material—Section S.I.; Scheme S1 and Table S1), it can be used for all of the applications listed above and not just for synthesis purposes. While polymers are both natural and synthetic, one of the important characteristics of polymers is the fire safety aspects, and this especially applies to synthetic ones. The production of synthetic plastic resins increases enormously year by year, and the U.S.A.’s consumption constitutes about one quarter of worldwide plastic consumption, followed by the European Union and Japan [13] (pp. 2–6). All organic polymers are combustible. They decompose when exposed to heat, their degradation products burn, smoke is generated, and the products of combustion are highly toxic. The prime toxic product is CO in concert with CO₂. Fire performance is not a single material property and is regulated by many material parameters. Fire behavior of materials combines the ease of thermal degradation, ease of ignition, flame spread, heat release, ease of extinction, smoke generation, toxic potency and other properties. While there are some polymers that are very difficult to ignite or consume with flames, most other polymers require flame-retardant additives to pass regulatory tests required for the safe use and sale of polymeric material-containing goods [13] (pp. 2–6). With this background in place, one can see that research on the fire safety of polymers has an important role to play in modern society. This volume is about the latest research at the intersection of the fields of fire and polymers, with a strong focus on material chemistry. Therefore, this study is strictly directed towards understanding the partial combustion properties or, more precisely, the thermo-oxidative degradation properties (not in pure O₂ but in the air as a reaction atmosphere) of strong ion-exchange resin (*p*-alkoxy-benzyl alcohol polymer-bound–Wang resin) as well as conducting a detailed kinetic analysis, enabling the validation of reliable mechanistic schemes that govern pathways in the oxidative degradation of the investigated type of resin. The thermo-oxidative behavior and kinetic degradation mechanism of [4-(hydroxymethyl)phenoxyethyl]polystyrene resin in an air atmosphere are not described in the literature, and therefore, there are no data attached to these issues. There are no studies that have dealt with the identification of products generated from the thermo-oxidative degradation process of the studied resin and obtained on the basis of the application of model-free and model-based kinetic methods. Therefore, the examination of the process in simulated adiabatic conditions for a thermal risk assessment represents

an unmistakable novelty and highlight of this research. This article allows readers to learn about the possibilities of the thermal separation and synthesis of important chemical compounds and the location of potential hazardous species when this resin is exposed to oxidative degradation conditions, especially in reactor-type facilities (considering that the examined resin comprises organic matter, this beckons critical (chemical) assessments with respect to combustibility, resistance to fire and gas formation).

In this work, all kinetic calculations were carried out using Kinetics Neo computational software (NETZSCH Kinetics Neo, product version: 2.6.6.7; build date: 16 November 2022) [14]. The current research is divided into five parts: (a) first, an analysis of the general thermo-oxidative characteristics related to resin stability and thermal effects that appear during the thermo-oxidative process; (b) second, a model-free analysis of the process and physicochemical description of its kinetic complexity; (c) third, a model-based kinetic analysis of the process and mechanistic explanation of the entire process, with appropriate descriptions of the kinetic models attached to the individual reaction steps (under the c) within the mechanistic explanation, and the role of mass transfer limitations in the synthesis of chemicals during the thermo-chemical conversion of the resin is discussed in the occurrence of “flow” chemistry, which is essential in the case of chemical reactors; (d) fourth, a comparison of the degree of conformity between the model-free and model-based results, which should result in setting up a realistic reaction mechanism of the studied process; and finally, (e) an extended investigation related to assessing the thermal safety of the chemical process, using adiabatic 24 h simulation tests, which are conducted with a differential scanning calorimeter (DSC) or an accelerating rate calorimeter (ARC). These predictions were performed under strict adiabatic conditions for the given parameters, with a pre-defined time to maximum reaction rate (e.g., 24 h), including the applied methods/models. The established results from the applied simulations were also discussed from the standpoints of heat and mass transfer effects. All the conducted tests and obtained results related to this type of polymer resin are reported in this work for the first time.

2. Materials and Methods

2.1. Material

Details about the used material in this work can be seen in Supplementary Material (Scheme S1 and Table S1 within Section S.I).

2.2. Simultaneous Thermal Analysis (TGA-DTA) Measurements of the Resin’s Thermo-Oxidative Degradation

Thermogravimetric analysis (TGA) and differential thermal analysis (DTA) measurements were performed with a TA Instruments SDT 2960 Simultaneous TGA-DTA analyzer, manufactured by TA Instruments (159 Lukens Dr, New Castle, DE 19720, UK). Pieces of the tested resin, i.e., the resin pearls weighing 4–5 mg, were placed in an aluminum crucible inside the TGA-DTA analyzer, with air as the purged gas with a dynamic air flow of $\varphi = 40 \text{ mL/min}$. Samples were heated from 30°C up to 800°C under a linear heating program at the heating rates of $\beta = 5, 10, 20$ and 30 K/min . All experiments were repeated at least three times. The temperature reproducibility of the instrument is $\pm 1^\circ\text{C}$, while the mass reproducibility is $\pm 0.2\%$. The TA Instruments SDT 2960 device operates with Universal Analysis Software which allows one to analyze the data from various thermal analysis techniques, simultaneously converting a TG signal into its derivative form (as a DTG curve at each heating rate used).

2.3. Thermo-Oxidative Characteristics Indices and Kinetic Methods

A detailed insight into the description of the characteristic indices of the thermo-oxidative degradation process, as well as the theoretical backgrounds related to the applied kinetic approaches in this study, can be seen in the Supplementary Material (Sections S.II and S.III).

3. Results and Discussion

3.1. Thermal and Thermo-Oxidative Properties

Figure 1a shows TGA curves of the thermo-oxidative process of the studied polystyrene resin at different heating rates in an air atmosphere. From Figure 1a, it can be clearly seen that there are four regions with different mass losses of the sample, namely, first, $\Delta m_1 \sim 3.44\%$, second, $\Delta m_2 \sim 23.06\%$, third, $\Delta m_3 \sim 44.60\%$, and fourth, $\Delta m_4 \sim 28.71\%$, respectively. It is evident that the reaction profile of the tested resin is very complex. Based on the TGA/DTA data, it can be seen that degradation chemistry represents a mixture of complex reactions, with different thermal effects (Figure 1b). The first mass loss step (3.44%) matches the moisture evaporation from the resin surface (characterized by the small endothermic effect that occurs till $100\text{ }^{\circ}\text{C}$) [15]. The specified mass loss of the sample also includes the volatilization process of divinylbenzene (DVB) since the resin is cross-linked with 1% DVB (“resin softening”) [15]. This process occurs in a temperature range of approximately $\Delta T \sim 100\text{--}210/220\text{ }^{\circ}\text{C}$, without notable thermal effects (Figure 1b, stage “I”). In this case, it is possible that the eventual initial endothermicity is masked by the high exothermicity of the process, initially slower, of significantly lighter resin fractions and later by an increasingly rapid process, related to heavy resin residues. Namely, the temperature ranges between $100\text{ }^{\circ}\text{C}$ and $220\text{ }^{\circ}\text{C}$ can be attributed to the transformation initiated by the reaction of residual double bonds in the DVB/PS-supported resin core [15]. The second mass loss step (23.06%) (Figure 1a) covers the temperature range between $220\text{ }^{\circ}\text{C}$ and approx. $350\text{ }^{\circ}\text{C}$, which is characterized by an exothermic event, whereby exothermicity increases slightly with higher temperatures ($\sim 310\text{ }^{\circ}\text{C}$, Figure 1b, stage “II”). This stage can be attributed to cracking reactions, where reactive radical species may be involved and whereby combustible compounds could be generated [16]. Next, the third mass loss, which is also the largest (44.60%) (Figure 1a), takes place between $350\text{ }^{\circ}\text{C}$ and approx. $450\text{ }^{\circ}\text{C}$, and this stage is characterized by an endothermic effect ($\sim 400\text{ }^{\circ}\text{C}$, Figure 1b, stage “III”). The observed stage corresponds to an oxygen–polymer interaction, i.e., oxygen reacts with polystyrene (PS) and its degradation products, yielding the char product. Namely, oxygen initiates depolymerization, which leads to the formation of hydro-peroxides that can yield char [17].

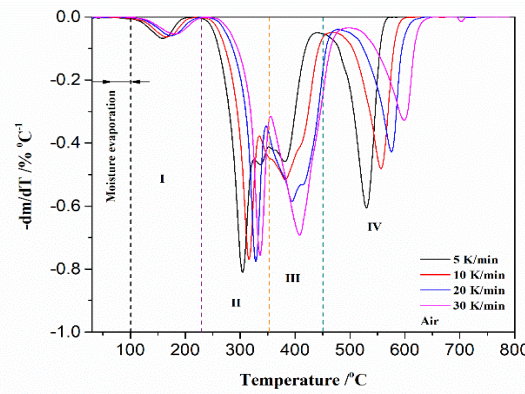
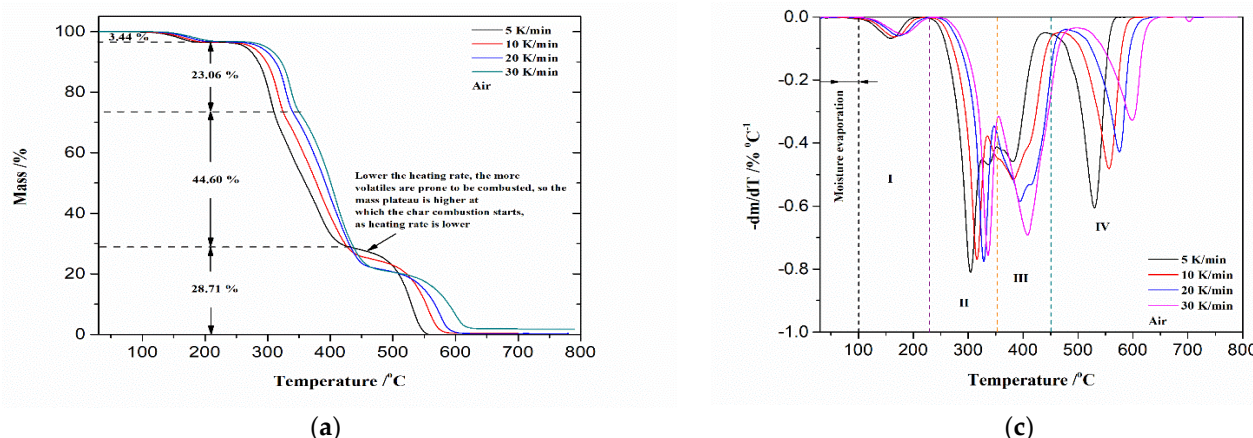


Figure 1. Cont.

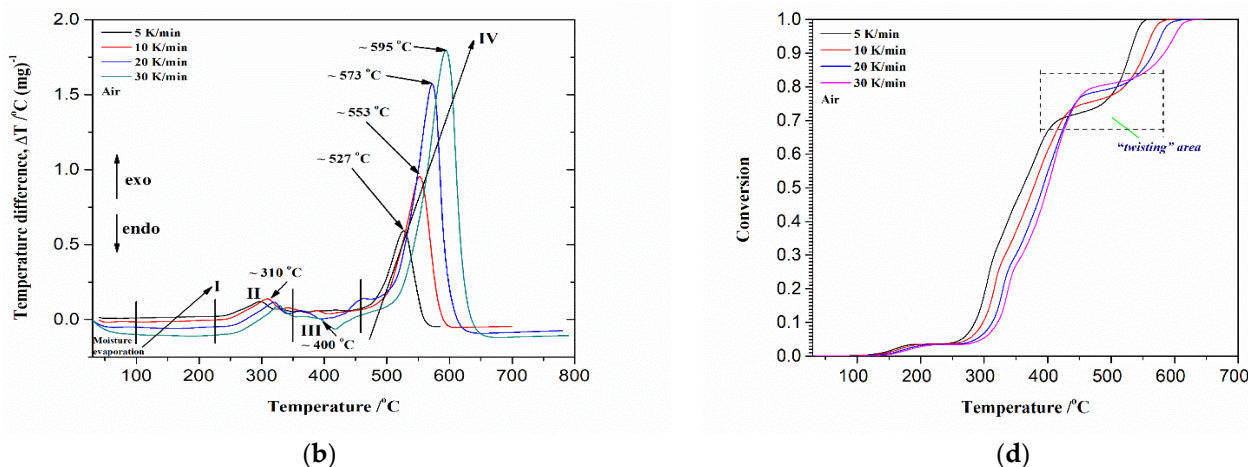


Figure 1. (a) TGA curves of [4-(hydroxymethyl)phenoxyethyl] polystyrene resin thermo-oxidative degradation process at different heating rates (5, 10, 20 and 30 K/min) (corresponding mass losses of the sample regarding the process stages are indicated), (b) DTA curves of [4-(hydroxymethyl)phenoxyethyl] polystyrene resin thermo-oxidative degradation process at different heating rates (5, 10, 20 and 30 K/min) (the appropriate thermo-oxidative stages (except for the stage related to moisture evaporation) are indicated by “I, II, III and IV”; the positions of some of the specific reaction temperatures are also indicated), (c) DTG curves of [4-(hydroxymethyl)phenoxyethyl] polystyrene resin thermo-oxidative degradation at different heating rates (5, 10, 20 and 30 K/min) (the markings on the graph are valid, as previously indicated), and (d) conversion–temperature ($\alpha - T$) reaction profiles at the heating rates of $\beta = 5, 10, 20$ and $30 \text{ K}/\text{min}$ (the phenomenon of “twisting” area emergence is clearly marked) [note: the y -axis in Figure 1c is expressed in $\% \cdot ^\circ C^{-1}$ and represents directly the first derivative of TGA curve, so actual curves belong also to the TGA analysis; the mass change per degree Celsius shows the temperature where the maximum change in the mass happens in the sample, so the slope and the height of the sample changes per degree Celsius in the graph are comparable if different heating rates exist—curve showing mass change per degree Celsius means dm/dT , which is called DTG curve, but it can be manually drawn as dm/dt from TGA curve, using simpler software [18].

The volatile products formed by degrading the hydro-peroxide groups are phenol, benzaldehyde and acetophenone [19]. In accordance with McNeill et al. [20], the main products of PS thermo-oxidative degradation were styrene, CO_2 , H_2O , benzaldehyde, α -methylstyrene, phenol, phenylacetaldehyde and acetophenone.

Immediately after the mentioned reaction stage, there follows a stage characterized by the mass loss of the sample of 28.71%, especially for $T > 450 \text{ }^\circ \text{C}$, which shows a strong exothermic event with an enhanced effect as the heating rate increases (increase in T) (Figure 1b, stage “IV”). This results in a “disturbance” of TGA traces, and one of explanations for this phenomenon is explained in Figure 1a. Namely, in an air atmosphere, the heavier fraction together with the carbonized fraction burns before complete carbonization. The lower the heating rate, the more non-volatile fractions prone to degradation are created, and because of this, the mass percentage plateau at which degradation begins is a higher, as the heating rate is much lower. This effect can be seen in conversion (α)–temperature (T) curves (Figure 1d), where a “twisting” area is marked. The observed area represents a reaction zone, where the char degrades in the presence of oxygen. This indicates that in the current phase of the process, the char yield is dependent on the heating rate, β . During the char formation, within PS smoke features, styrene, benzaldehyde, naphthalene, propenylbenzene, and phenanthrene dominate [21]. Namely, the current reaction zone is characterized by a much faster escape of the volatiles, where a hysteresis effect is probably also present (a continuous increase in the temperature causes the tested sample to carry on oxidizing and degrade at a low heating rate, thereby suggesting apparently that the conversion degree seems similar to that at higher temperature degradation rates).

However, considering the above results, in the case of [4-(hydroxymethyl)phenoxyethyl] polystyrene resin degradation, the “intermediate” char is formed between $\alpha \approx 0.70$ and $\alpha \approx 0.80$ ($\Delta T \sim 425\text{--}520\text{ }^{\circ}\text{C}$; transitioned T-shift “III→IV”) and then degraded at higher temperatures (for $\alpha > 0.80$ and $T > 520\text{ }^{\circ}\text{C}$) (Figure 1a,d). Unlike the pure PS, in the case of the tested resin, the amount of the final residue is not zero, and the average (considering all heating rates) ultimate residue of $\Delta m_{\text{res}(\text{avg})} \sim 0.64\%$ is obtained (unburned residue in oxygen). Nevertheless, it can be observed that char yield forms immediately after the expiration of stage “III”, which might include competitive reactions, and is strongly dependent on the heating rate. It should be noted that diffusion processes may occur, i.e., oxygen diffusion into the micro-pores of carbon-based material can speed up considerably at high temperatures, causing a large release of gaseous products (primarily CO_2 and H_2O) in the “carbonization” stage (which may generate a significant amount of unburned hydrocarbons, formed during the course of resin conversion, and then they degrade and oxidize into gases).

Along with the presented results confirming the existence of complex reactions that occur during thermo-oxidative processes, corresponding DTG curves at different heating rates are shown in Figure 1c. Furthermore, a visual inspection of thermo-analytical curves often indicates that the overall process contains more than one reaction step and can aid the detection of the multi-step nature of a process, which lies behind it. The visual inspection is more effective when we apply the absolute conversion rate curves ($\% \cdot \text{min}^{-1}$) (Figure 1c), and they are shown in Figure 2.

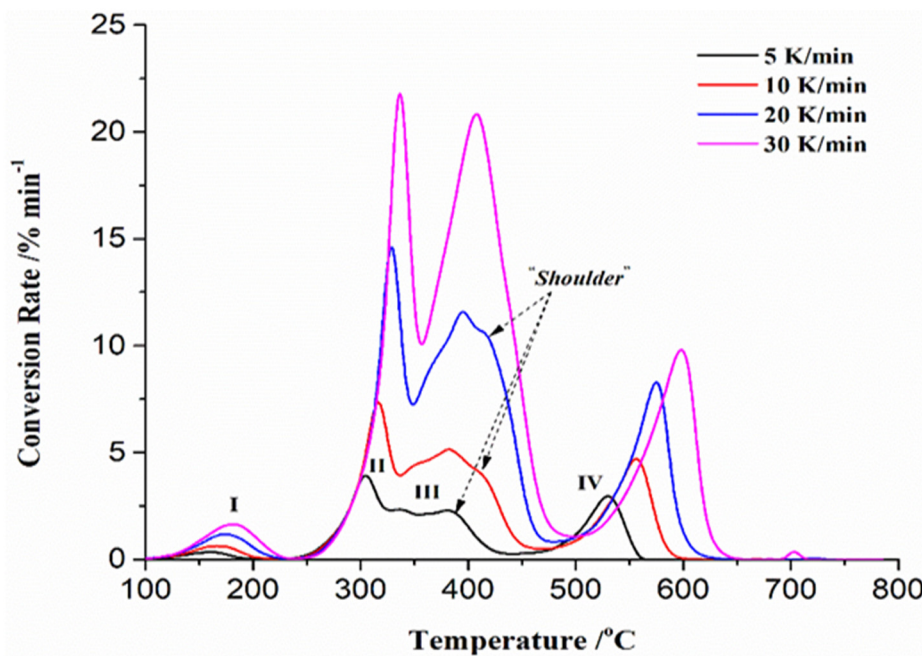


Figure 2. The absolute conversion rate ($\% \cdot \text{min}^{-1}$) curves against temperature (T) at different heating rates ($\beta = 5, 10, 20$ and 30 K/min) for thermo-oxidative process of [4-(hydroxymethyl)phenoxyethyl] polystyrene resin (as indicated earlier, the appropriate resin thermo-oxidative stages are designated “I, II, III and IV” (the moisture evaporation stage is not taken into account—it is excluded from further consideration); observed “shoulders” are indicated on the same graph) [note: the curves presented in Figure 2 represent derivative plots, expressed through conversion rates from non-isothermal curves shown in Figure 1d in absolute units as $\% \cdot \text{min}^{-1}$, with numerical values that of course differ from those presented in Figure 1c, and if these curves were presented in relative rate units, on the y -axis, the values would be in the range [0;1]—Figure 2 shows curves transferred from Kinetics Neo computational software 2.6.6.7 as output results].

As can be seen from Figure 2, the presence of several peaks and “shoulders” indicates the multi-step character of the studied thermo-oxidative degradation process. Since there

exists a set of single peaks (“at all heating rates”) with the detection of “shoulders”, consecutive and/or independent reaction steps can be expected (where an overlapping effect during the thermo-oxidative process may exist as well). It should be emphasized that at the highest heating rate (~30 K/min), the identified “shoulder” disappears, but the “shoulders” region occurs in the part of the process where the resin char yield is formed, suggesting its strong dependence on the heating rate—consequently due to the thermal expansion of the resin during the heating (see the above results). For further analysis, the moisture evaporation (dehydration) step was excluded, especially in the case of the kinetic analysis (see later).

3.2. Resin Thermo-Oxidative Degradation Performance Results

Table 1 shows thermo-oxidative degradation characteristic parameters for the tested resin (see Supplementary Material). Corresponding parameters were determined from Figure 1a,c.

Table 1. Thermo-oxidative characteristics of [4-(hydroxymethyl)phenoxyethyl] polystyrene resin at different heating rates.

β (K/min)	T_i (°C)	T_p (°C)	T_b (°C)	R_p (%·°C ⁻¹)	R_v (%·°C ⁻¹)	t_i (min)	t_p (min)	t_b (min)	$\Delta t_{1/2}$ (min)	$S \times 10^{-9}$ (% ² ·°C ⁻³)	C (%·°C ⁻³)	D_i (%·°C ⁻¹ ·min ⁻²)	D_b (%·°C ⁻¹ ·min ⁻³)
5	255	305	545	-0.835	-0.182	43	53	101	3.62	4.288	1.284×10^{-5}	3.664×10^{-4}	4.309×10^{-5}
10	270	315	575	-0.798	-0.150	23	27.5	53.5	1.54	2.856	1.095×10^{-5}	1.262×10^{-3}	3.522×10^{-4}
20	290	330	590	-0.806	-0.132	13	15	28	0.84	2.144	9.584×10^{-6}	4.133×10^{-3}	2.285×10^{-3}
30	295	335	615	-0.787	-0.128	8.83	10.17	19.5	0.54	1.882	9.043×10^{-6}	8.764×10^{-3}	7.349×10^{-3}

It can be seen from Table 1 that the ignition (T_i), maximum (peak) (T_p) and burnout (T_b) temperatures rise with an increase in the heating rate (there is also a lateral increase in these temperatures, considering individual heating rates), while the corresponding time values decrease. Since the tested resin is combustible, this resin is not easily flammable, i.e., it cannot ignite readily. Therefore, oxygen adsorption on the resin surface may facilitate early ignition and degradation. Consequently, after 250 °C, as the temperature increases, and beyond 300 °C, there is a great mass decrease due to the rapid resin thermo-oxidative degradation. The mass change continuously decreases with an increase in the temperature. Comparing T_i values, the tested resin has a lower T_i than the ignition temperature of the epoxy-diane resin (~305 °C) [22] and the ignition temperatures of some polymers, such as polyphenylenesulfide (PPS) (~528 °C), polybutyleneterephthalate (PBT) (~370 °C) and polycarbonate (PC) (~493 °C), as well as pure polystyrene (PS) (~356 °C) and polypropylene (PP) (~325 °C) [23]. Thus, the thermo-oxidative stability of the *p*-alkoxybenzyl alcohol resin appears to be lower than for the polymer systems listed above. Unlike some polymers and epoxy-based composites, this resin shows an increased reactivity of polymers chains in the process of thermo-oxidative degradation (t_i noticeably decreases with the heating rate elevating, so the large amount of thermal energy causes faster bond breakings). Considering T_p values (Table 1), where the main group of DTG peaks is located (Figure 1c), the thermo-oxidative intensity of these peaks is affected by the heating rate to a small extent (it should be noted here that this group of peaks attached to the T_p values is insensitive to the heating rate when it is expressed by %·°C⁻¹ (see Figure 1c) compared to those expressed by %·min⁻¹ (Figure 2)). However, as the temperature progresses, in the transition to process stage “III”, the intensities of the DTG peaks become significantly dependent on the heating rate, and this can be especially noted in the case of the last group of DTG peaks, considering the oxidative reaction of the carbonized residual. Hence, the pyrolytic residue of the organic constituents of the resin combusts in a narrower temperature range (Figure 1). In addition, with an increasing of the heating rate, T_b value increases in the range from 545 °C to 615 °C ($\Delta T_b = 70$ °C), where the fast heating may lead to quality “defects” due to intensive gas evolution during degradation. Namely, since burnout temperature increases with an increase in the heating rate, the rapid heating probably implies a larger thermal lag of resin particles, which may cause a longer completion time of the process. Considering

thermo-oxidative performance indices S , C , D_i and D_b (Table 1), the values of S and C decrease with an increase in β . Since the flammability index (C) represents the chemical reaction activity at the initial thermo-oxidative stage, the obtained results for C indicate that better combustion and ignition stability of the resin are achieved at low heating rates (a tendency towards lower temperature action). On the other hand, since index S reflects the integrated ignition and burnout performance of the tested resin, the results suggest that the best overall performance is achieved at the lowest heating rate (Table 1). At the fixed heating rate, the values of C are higher than S , so C prefers conditions where the flammability is much better and the flame of the resin is more stable during slower heating processes.

Among the four different heating rates applied, the most optimal heating rate is $\beta = 5 \text{ K/min}$. Consequently, the combustibility of the considered resin is closely related to its volatile characteristics. However, it should be noted that the ignition temperature is not only affected by volatile content but also by other factors, such as the heating rate, as noted earlier. In respect to the D_i and D_b indices, here, there is a different situation, where D_i and D_b values increase with an increase in the heating rate (Table 1). For both indices, the largest jump in values is recorded at the transition from 5 K/min to 10 K/min. Since both parameters (D_i and D_b) represent the intrinsic parameters, their data allow us to establish the optimal conditions for the thermo-oxidative process of the tested resin. It can be seen that D_i significantly increases when the heating rate exceeds 10 K/min. So, a faster rate of heating allows a large amount of the heat to be supplied for resin degradation in the initial stages, where the increase in the heating rate has a positive response to ignition behavior. Considering D_b , which is associated with t_b , it can be seen that the highest value of D_b is achieved at a heating rate of 30 K/min but with the lowest value of t_b (Table 1). This indicates that there is a faster heat and mass transfer rate, leading to "higher thermo-oxidative efficiency". There is a tendency that the higher ash content represents an important factor, which leads to low D_b value. The ash content after degradation process of the resin is still remains (Figure 1a), so temperature and pressure gradients between the upper and lower parts of the ash deposits probably exist, which can increase the resistance of the oxygen contact and thermal diffusion. This may result in a slower resin thermo-oxidative process. Since $D_b < D_i$ at all heating rates, the tested resin is characterized by relatively good thermal stability at the lowest heating rate, where its degradation becomes easier with an increase in β s. However, because of the exposed facts above related to the effect of the heating rate, the degradation of the resin at high heating rates is less complete than that at low heating rates.

Types of Functional Dependences of T_i , T_p and T_b on the Heating Rate

Figure S1 represents the functional relationships between T_i , T_p and T_b and the heating rate (β), where functionalities are expressed as $T_i \text{ [in K]} = f(\beta \text{ [in K/min]})$ (a), $T_p \text{ [in K]} = f(\beta \text{ [in K/min]})$ (b), and $T_b \text{ [in K]} = f(\beta \text{ [in K/min]})$ (c) (Supplementary Material). Considering the results shown in Figure S1a,b, for both temperatures, T_i and T_p , there is an excellent fit of dependence of these temperatures on the heating rate (adj. R-Square, $R^2 > 0.999$), with rational power functions that include similar values to the fitting parameters. The best selected function is the thermal degradation behavior function (TDBF) for the dependence of T_i and T_p on the heating rate established for the tested resin.

Given polynomial propagation regarding the heating rate, which involves the functions presented in Figure S1a,b, the rise in temperature leads to the diminution in resin thermal stability. This can be reflected through the decrease in the initially predominant cyclic structure's species within the investigated resin. Deviations from linearity and the transition to the curvature relationship of T_i/T_p against β could be an indication of the thermal variations in PS oligomers, which may be affected by the heterogeneity of the studied material, weakening its polymeric structure. On the other hand, in the case of the dependence of the burnout temperature (T_b) on the heating rate (β), the experimental points do not show some of the regular trends with β s (Figure S1c). There is a poor fit with the best

selected (exponential) function ($R^2 = 0.88467$) (if compared with cases for temperatures T_i and T_p), while the linear relationship gives a slightly better quality of the fit ($R^2 = 0.91043$) (Figure S1c). Despite these fitting procedures, both functions give high temperature values for important fitting parameters, $a = 906.35$ K per exponential function and $a^* = 812.81$ K per linear function, respectively. Both values belong to the temperature range where strong exothermic effects occur (stage “IV”, Figure 1b). In thermo-oxidative conditions, this large exothermic effect results from the combustion of gases evolved during the process, as well as the “secondary” degradation of polycyclic aromatic compounds (PAHs) formed from the destruction of most of the polymer’s structure. In this context, the process itself “forces” the use of a high heating rate ($\beta_c = 32.82$ K·min⁻¹, Figure S1), resulting in the release of a large amount of heat, which, as previously noted, leads to the destabilization of the process, especially at the end of it. This phenomenon is directly reflected in T_b temperature behavior by its drastic expansion (see Table 1, where $\Delta T_b \sim 70$ °C), without a strong and specific functional dependence on the heating rate. These results are in good agreement with the previous ones. Consequently, changes in the heat release rate can influence the mass loss history of the resin (Figure 1a) and thus will unambiguously affect the kinetic nature of the mechanism of the process.

3.3. Kinetic Modeling of Thermo-Oxidative Degradation Process

3.3.1. Results of Multiconversional Dependent Analysis—Model-Free Kinetics

Based on the model-free methods described in the Supplementary Material, $E_a(\alpha)$ curves of the studied resin thermo-oxidative process were obtained. Figure 3 shows E_a -conversion profiles, using Friedman (FR), Vyazovkin (VY) and numerical (NM) (optimization) models, respectively. As can be seen from Figure 3, all model-free models show an identical trend of the change in the effective activation energy (E_a) values with the conversion.

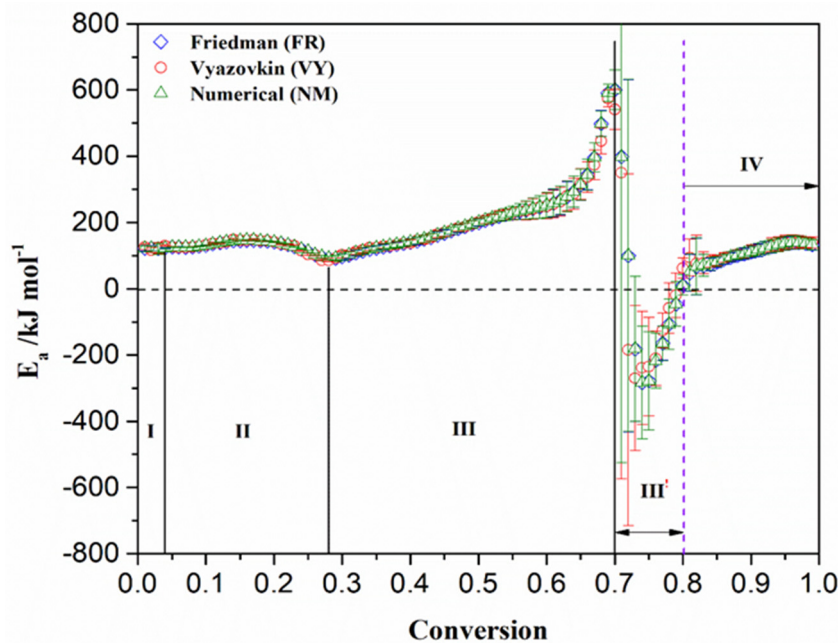


Figure 3. Multi-conversional dependent effective activation energies ($E_a(\alpha)$) obtained by Friedman (FR), Vyazovkin (VY) and numerical (NM) methods for the thermo-oxidative process of [4-(hydroxymethyl)phenoxy]methyl] polystyrene resin.

The results obtained through the application of Friedman (FR), Vyazovkin (VY) and numerical (NM) models clearly indicate the extraordinary kinetic complexity of the studied process, which manifests a multi-step reaction character. Since E_a exhibits strong variation with conversion (α), here, the single, the constant set of the kinetic triplet, from standard

kinetic description of the process does not appear, but the variation in effective activation energy values with the progress of the reaction exists. From Figure 3, it can be seen that we have five areas where the E_a changes with conversion, but the magnitudes of these changes are not the same across the regions, and the areas are marked “I, II, III, III^l, and IV”.

Taking into account the actual trends, which are valid for the changes in E_a values with α (Figure 3), in each of the mentioned areas, it is possible to draw the following conclusions (for an example, considering the FR data, but the situation is very similar to the data of the other two methods):

- (1) At low conversions ($\alpha = 0.01\text{--}0.04$), there is an almost constant value of the E_a with a negligible variation with α (area I) ($\Delta E_a = 122.107 \text{ kJ}\cdot\text{mol}^{-1}\text{--}123.088 \text{ kJ}\cdot\text{mol}^{-1}$). There is only one reaction in this area, the single-step reaction of type A→B.
- (2) With the increase in conversion, in area II, which includes $\alpha = 0.05\text{--}0.28$ (Figure 3), there is a gradual increase in the value of the E_a ($\Delta E_a = 125.88 \text{ kJ}\cdot\text{mol}^{-1}\text{--}145.641 \text{ kJ}\cdot\text{mol}^{-1}$), reaching a local maximum (at $\alpha \sim 0.16$ for $E_a = 146.146 \text{ kJ}\cdot\text{mol}^{-1}$), and then a slightly faster decrease ($\Delta E_a = 145.857 \text{ kJ}\cdot\text{mol}^{-1}\text{--}92.026 \text{ kJ}\cdot\text{mol}^{-1}$), until the conversion of $\alpha \sim 0.29$. In this part, the process becomes kinetically complicated. A sequential type of reactions (mostly consecutive) composed of two successive simple reactions of type C→D→E can appear here, where each reaction in the sequential step is characterized by different activation energy values ($E_1 \neq E_2$) related to the individual steps.
- (3) After $\alpha \sim 0.29$, until $\alpha = 0.70$ (within area III), there is a progressive increase in the activation energy from $E_a = 92.026 \text{ kJ}\cdot\text{mol}^{-1}$ to $E_a = 313.456 \text{ kJ}\cdot\text{mol}^{-1}$ (in the conversion range between $\alpha = 0.29$ and $\alpha = 0.65$) and then a sudden jump in E_a to a maximum value of $E_a = 600.773 \text{ kJ}\cdot\text{mol}^{-1}$ (Figure 3). In this part, the resin degradation process is further complicated, where parallel reactions [24] can be expected, but which type is difficult to determine. This especially applies to whether some of them are consecutive or single-step reactions. Competition between the individual steps cannot be ruled out here either. This part of the thermo-oxidative process can hardly be resolved from this point of view. On the other hand, what type of kinetic model is involved is also difficult to determine from the established $E_a(\alpha)$ profiles. So, considering the obtained $E_a(\alpha)$ dependency, the model-free method's capabilities are limited because they cannot answer all questions related to thermo-oxidative degradation kinetics. Drawing the full mechanistic conclusion is critical here. Namely, in this specific case, what cannot be distinguished is the appearance of autocatalytic and non-self-accelerating reactions (namely, autocatalytic reactions are often described by a single value of E , as well as a simple reaction of the n -th type. Therefore, for the single-step reaction, E will always be constant irrespective of the specific reaction mechanism). But in addition to this, in order to obtain a quality kinetic prediction of the considered process, the knowledge of $A(\alpha)$ profiles is the necessary, i.e., giving us the opportunity to predict the reaction rate values (see later results).
- (4) In the next area, marked III^l, there is a serious disturbance in the change ‘signal’ in the E_a values with conversion that exists in a narrow α -range ($\alpha \approx 0.71\text{--}0.80$) (Figure 3). There is a sudden drop in the E_a value towards the negative sign and then an increase with the retention of a negative (high) value, until near $\alpha \approx 0.80$. Since the E_a value decreases sharply, and it is negative, this suggests that the mass loss rate decreases as the temperature further increases. Indeed, in Figure 1c, it can be seen that within stage IV, the higher mass loss rate is observed at lower heating rates compared to higher heating rates. This indicates that the current reaction segment of the resin's thermo-oxidative process manifests a negative dependence on the temperature. In the studied case, within zone III^l (Figure 3), the applied model-free models fail to provide any trustable mechanistic information [25]. However, from a purely phenomenological aspect, this phenomenon could be interpreted as a barrierless reaction step or where an oxidative reaction proceeds spontaneously. A possible explanation for this lies in the initial stage of the polymer support degradation of the resin. Namely, it is evident that stage II is exothermic (Figure 1b), so the heat released during this stage of the

polymer degradation was not taken into account in Equation (S12) (Supplementary Material) for the calculation of activation energy values. Therefore, the heat released here is apparently sufficient to start the processes of char degradation, releasing even more heat. Likewise, in the last case, radical–molecule reactions should not be excluded from the participation. Namely, these reactions are nonelementary reactions, which may exhibit negative activation energies, which usually proceed through two steps. These reactions can often exist in atmospheric chemistry and in the hydrocarbons' thermo-oxidative degradation. As a consequence of the mentioned factors, the isoconversional principle was not held at all, but on the other hand, this confirms the dependence of the evolution on the specific thermal history of the combusted system.

- (5) After area III¹, there is an increase in an effective activation energy with conversion (area IV), with positive E_a values (from approx. $48.537 \text{ kJ}\cdot\text{mol}^{-1}$ to $139.182 \text{ kJ}\cdot\text{mol}^{-1}$ for $\alpha \approx 0.81\text{--}0.97$), until the very end of the process (where a slight drop in the E_a value is observed from $136.801 \text{ kJ}\cdot\text{mol}^{-1}$ at $\alpha = 0.98$ to $132.705 \text{ kJ}\cdot\text{mol}^{-1}$ at $\alpha = 0.99$). This can be attributed to the secondary cracking process of polycyclic aromatic hydrocarbons (PAHs), arising from the thermal destruction of the PS polymer structure [26], as well as thermal damage of the Wang linker structure (Scheme S1), which probably happened much earlier, probably in the III area.

Using the procedure described in the Supplementary Material, $\log A(A/\text{s}^{-1})$ –conversion dependency is determined by Friedman (FR), Vyazovkin (VY) and Numerical (NM) methods, respectively. The $\log A(\alpha)$ profiles for the studied thermo-oxidative process are shown in Figure S2 (Supplementary Material).

As can be seen from Figure S2, the obtained $\log A(\alpha)$ profiles show an identical trend with α , as well as $E_a(\alpha)$ profiles, thus confirming the multi-step (complex) nature of the investigated process. Considering the narrow α -range where the negative $\log A$ values occur, there are very small pre-exponential factors, which bring about an extremely high term, $\exp(-E_{a,\alpha}/RT_\alpha) \approx \times 10^{15}$. This results in a drastic decrease in the rate constant with increasing temperatures, i.e., it has a negative temperature dependence; or in other words, the rate decreases with an increase in the temperature. This can happen if a such type of reaction consisting of the rate-determining step exists with an intermediate species.

Namely, the rate-determining step must have a positive temperature dependence, but the preceding equilibrium which produces an intermediate species could have a negative temperature dependence, affecting the overall reaction. Namely, this obviously occurs in the considered multiple-step process, where one of the reaction steps is endothermic (absorbs the heat). So, in a such case, the increase in the temperature actually can slow down the rate of the endothermic step, leading to an overall decrease in the rate of reaction. However, there may be a case when the rate of reaction decreases with the temperature in an event involving the reaction catalyzed and the catalyst is de-activated at higher temperatures. Since the above-described case belongs to the segment of the process where a strong exothermic event takes place, the actual discussion of it can be too general, but it can be specified considering what conditions the observed reaction proceeds. This may be accompanied by additional effects, primarily the transport phenomena (see later discussions). In the case of the presence of autocatalytic reactions, the rate can increase and then decrease. Consequently, the additional increase in the temperature can results in a temporary decrease in its rate.

Further on, the deviation of the E_a from its mean value, $E_{a(\text{mean})}$, for all the applied model-free methods was determined, using the following equation:

$$\varepsilon_m(\%) = 100 \cdot \frac{|E_a - E_{a(\text{mean})}|}{E_{a(\text{mean})}}, \quad (1)$$

where ε_m represents the deviation in percentages, while $E_{a(\text{mean})}$ is the mean effective activation energy value, which was extracted for each of the applied model-free methods (FR, VY and NM) (there are possible parallel and independent reactions).

Figure S3 (Supplementary Material) shows the ε_m (in %) against the conversion (α) for the Friedman (FR), Vyazovkin (VY) and numerical (NM) kinetic data in the case of the thermo-oxidative degradation process of [4-(hydroxymethyl)phenoxyethyl] polystyrene resin. As can be seen from Figure S3, in the case of all considered methods, the very large errors occur in the conversion range of $\Delta\alpha = 0.65\text{--}0.80$. Therefore, this means that the non-determinacy of the estimated E_a values in this conversion range is a very high. This lower accuracy can be attributed to pitfalls which are described above, regarding the model-free data, in a specified conversion range (the physical reasons were indicated earlier). However, since they were estimated in the 95% confidence limit, the E_a values can be credible in the observed conversion range, except for those with a large negative E_a value. In this context, this particularly applies to E_a s where their extreme variation with the conversion (considering all applied methods) can be seen (see Figure 3). Everything stated here confirms the very complex kinetic nature of thermo-oxidative degradation, which includes an undeniable existence of the multi-step reactions (previously defined and confirmed—see also the discussion above).

Results of the Statistical Analysis Related to Suitability of the Applied Model-Free Methods

For optimization and curve-fitting, the Kinetics Neo 2.6.6.7 software uses the non-linear least-square approach. In order to achieve the best coefficient of determination (R^2) in the calculations that fit the experimental data, the kinetic parameters are optimized, using the least-squares method. The F-test was chosen as a statistical test to compare the models and to assess the suitability of various model-free methods (FR, VY and NM), as well as for the model-based approach (see later).

For the statistical analysis, beside the best coefficient of determination (R^2) and the F-test, the sum of dev. squares (S^2), mean residual (MS) and Student's coefficient of 95% confidence intervals are also used. Details about these statistical quantities can be found elsewhere [27–29] (pp. 1–668). Table 2 shows the comparative statistical analysis results of different model-free models/methods (FR, VY and NM) for the thermo-oxidative degradation process of [4-(hydroxymethyl)phenoxyethyl] polystyrene resin.

Table 2. Comparative statistical analysis results (the statistical fit quality) of different model-free models (FR, VY and NM).

Method/Model	Fit to	R ²	Sum of Dev. Squares	Mean Residual	Student's Coef. 95%	F-Test
Friedman (FR)	TGA signal	0.98328	25,824.418	3.664	1.968	53.117
Vyazovkin (VY)	TGA signal	0.98173	28,200.346	3.664	1.968	58.004
Numerical (NM)	TGA signal	0.99688	4857.802	1.520	1.968	9.992

Considering the values of the obtained statistical parameters (Table 2), the FR and VY methods show a similar quality of fitting of their data to the experimental ones, with the fact that the FR method is slightly better in the observed case's. Namely, the higher R^2 value is withdrawn from the lower F-test value and the lower sum of the dev. square, indicating a good fit mode. Consequently, the NM method shows the best fit to the experimental data, so the following sequence of the models'/methods' fit qualities occurs: NM > FR > VY. The conversion-dependent fit curves related to the experimental TGA signals are shown in Figure 4a–c for the FR, VY and NM methods, respectively.

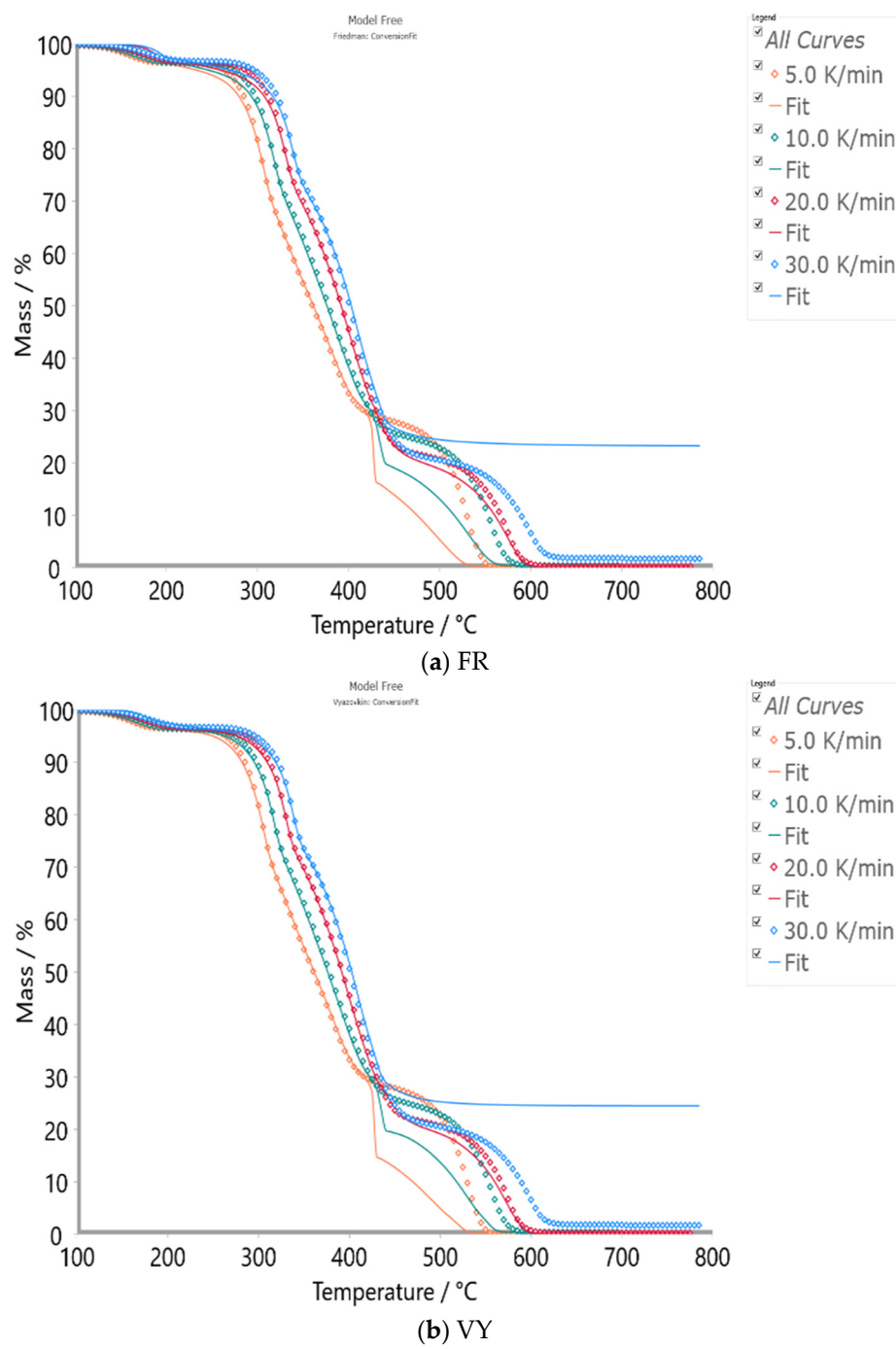


Figure 4. Cont.

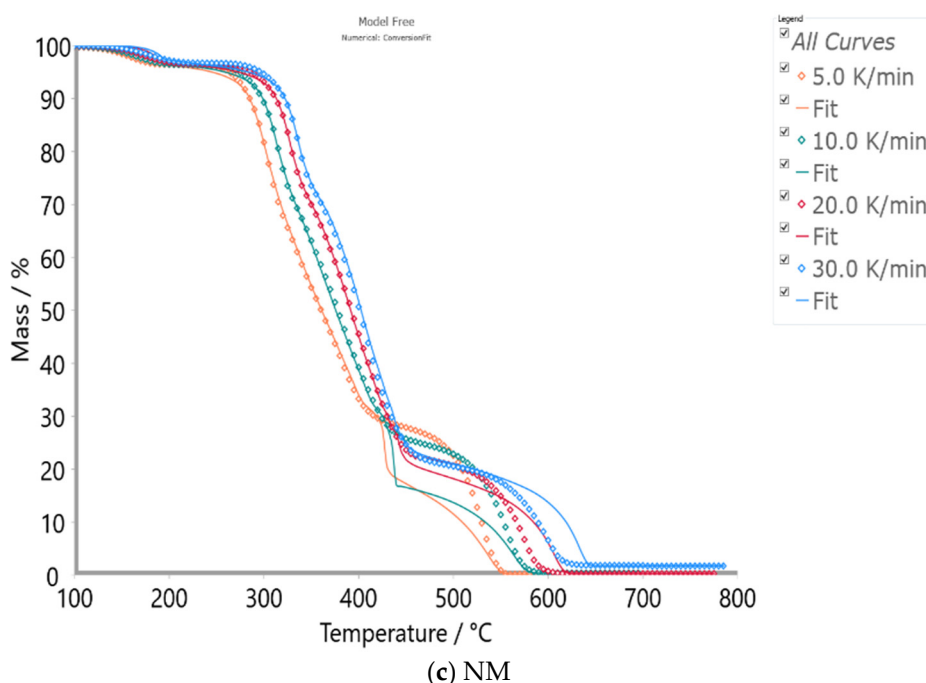


Figure 4. The “conversion-dependent” model-free data fit to the experimental TGA signals at the different heating rates (5, 10, 20 and 30 K/min) for (a) Friedman (FR), (b) Vyazovkin (VY) and (c) numerical (NM) methods in the case of the complex (multi-step) thermo-oxidative process of [4-(hydroxymethyl)phenoxyethyl] polystyrene resin.

As can be seen from Figure 4, all three methods/models show a high quality of fit to the experimental thermo-analytical data, up to the part of the process related to the char’s behavior and the additional thermal cracking of the solid residue (at all heating rates, for $T > 450$ °C, and especially for the conversion segment between $\alpha = 0.71$ and $\alpha = 0.83$). However, much better agreement between the fit values at all heating rates is shown via the NM method compared to the other two methods (Figure 4). This is clearly reflected in the values of the statistical quantities, shown in Table 2. So, looking at results obtained, the kinetic parameters estimated by the NM method can be used as the zero approximation for solving the resin thermo-oxidative mechanism scheme via the model-based kinetic approach.

The problem with the isoconversional approach here is that methods such as Friedman’s and Vyazovkin’s are much more “vulnerable”, where the degradation process exhibits different heat peak directions (apropos of the endo/exo effects, where exothermicity dominates at higher temperatures, i.e., including higher heating rates, as shown in Figure 1b), as well as where there is a certain “diversity” in the final mass loss (see, for example, the formation of the ultimate mass loss plateau in Figure 4, where at the highest heating rate (regarding the experimental data), this plateau was raised (showing the influence of the heating rate)). However, considering the numerical optimization, this method overcomes these problems much better, giving quite satisfactory results ($R^2 > 0.995$). Due to the large number of the kinetic equations and parameters available in the software (for the model-based analysis), there can be numerous combinations, which yield satisfactory results. Therefore, it is important to ensure that the correlation coefficient, such as R^2 , is very high, ideally, around the value $R^2 = 0.999$.

Prior to the application of the model-based analysis, the preliminary determination of reaction model types involved in the degradation mechanism based on Friedman’s (FR) isoconversional plots is explained and discussed in the Supplementary Material (Section S.IV; see Figures S4 and S5).

3.3.2. Model-Based Kinetics Analysis

Over multiple rounds of the MVNLR calculation simulations, the reaction scheme that best described the entire thermo-oxidative process was established, and it was coded with hx; model. This mechanistic scheme includes two parallel consecutive reaction steps and two independent single-step reactions, and this is shown through Equations (2)–(5) (note: the reaction scheme does not include the stage with moisture evaporation, omitted from the analysis for $T < 100^\circ\text{C}$).



In Equations (2)–(5), A, D, G and I represent the reactants and B and E are intermediate species, while C, F, H and J represent the products. The first sequential stage includes, for step $A \rightarrow B$, the n -th order chemical reaction (Fn) (Supplementary Material) and then, for step $B \rightarrow C$, the reaction of the n -th order with m -power autocatalysis by product (Cnm). The second sequential stage includes, for step $D \rightarrow E$, the Jander three-dimensional diffusion ($D3$), while for step $E \rightarrow F$, the three-dimensional nucleation (Avrami–Erofeev) model ($A3$) exists. The single-step reaction $G \rightarrow H$ proceeds via first-order autocatalysis ($C1$). Finally, the second independent single-step reaction $I \rightarrow J$ takes place through the two-dimensional nucleation (Avrami–Erofeev) model ($A2$) (Supplementary Material).

The corresponding rate law equations, which include the kinetic triplets for each reaction of the resin thermo-oxidative mechanism (Equations (2)–(5)), are given by Equations (6)–(11):

$$\text{Step : } A \rightarrow B / \text{Reaction type : } Fn, \frac{d(a \rightarrow b)}{dt} = A \cdot a^n \cdot \exp\left[-\frac{E}{RT}\right], \quad (6)$$

$$\text{Step : } B \rightarrow C / \text{Reaction type : } Cnm, \frac{d(b \rightarrow c)}{dt} = A \cdot b^n \cdot [1 + \text{AutocatPreExp} \cdot c^m] \cdot \exp\left[-\frac{E}{RT}\right], \quad (7)$$

$$\text{Step : } D \rightarrow E / \text{Reaction type : } D3, \frac{d(d \rightarrow e)}{dt} = A \cdot 1.5 \cdot \frac{d^{2/3}}{(1 - d^{1/3})} \cdot \exp\left[-\frac{E}{RT}\right], \quad (8)$$

$$\text{Step : } E \rightarrow F / \text{Reaction type : } A3, \frac{d(e \rightarrow f)}{dt} = A \cdot 3 \cdot e \cdot [-\ln(e)]^{2/3} \cdot \exp\left[-\frac{E}{RT}\right], \quad (9)$$

$$\text{Step : } G \rightarrow H / \text{Reaction type : } C1, \frac{d(g \rightarrow h)}{dt} = A \cdot g \cdot [1 + \text{AutocatPreExp} \cdot h] \cdot \exp\left[-\frac{E}{RT}\right], \quad (10)$$

$$\text{Step : } I \rightarrow J / \text{Reaction type : } A2, \frac{d(i \rightarrow j)}{dt} = A \cdot 2 \cdot i \cdot [-\ln(i)]^{1/2} \cdot \exp\left[-\frac{E}{RT}\right], \quad (11)$$

where A and E represent the pre-exponential factor (s^{-1}) and activation energy ($\text{kJ} \cdot \text{mol}^{-1}$) of the individual reaction steps. The corresponding mass balance equation is expressed as follows:

$$\text{Mass} = m_0 - \Delta m \times \left[ct_{tb}.(a \rightarrow b) \times \int \left[\frac{d(a \rightarrow b)}{dt} \right] dt + ct_{tb}.(b \rightarrow c) \times \int \left[\frac{d(b \rightarrow c)}{dt} \right] dt + ct_{tb}.(d \rightarrow e) \times \int \left[\frac{d(d \rightarrow e)}{dt} \right] dt + ct_{tb}.(e \rightarrow f) \times \int \left[\frac{d(e \rightarrow f)}{dt} \right] dt + ct_{tb}.(g \rightarrow h) \times \int \left[\frac{d(g \rightarrow h)}{dt} \right] dt + ct_{tb}.(i \rightarrow j) \times \int \left[\frac{d(i \rightarrow j)}{dt} \right] dt \right], \quad (12)$$

where m_0 is the initial mass, the quantity Δm represents the total mass change, and finally, ct_{tb} represents the contribution.

The values of the kinetic parameters and kinetic models in each kinetic triplet for the individual steps, together with the corresponding kinetic exponents and the contribution of each reaction step, for the overall thermo-oxidative process are listed in Table 3.

Table 3. Results of model-based kinetic analysis for [4-(hydroxymethyl)phenoxyethyl] polystyrene resin thermo-oxidative degradation process.

Model Scheme:	
	A–B–C
	D–E–F
	G–H
	I–J
Step: A→B. Reaction type Fn	
Activation energy, E (kJ·mol ⁻¹)	289.535
$\log A$, A (s ⁻¹)	22.507
Reaction order (n)	5.810
Contribution	0.208
Step B→C. Reaction type Cnm	
Activation energy, E (kJ·mol ⁻¹)	190.668
$\log A$, A (s ⁻¹)	13.182
Reaction order (n)	1.764
$\log(\text{AutocatPreExp.})$	1.508
Autocat. power (m)	8.131
Contribution	0.241
Step: D→E. Reaction type D3	
Activation energy, E (kJ·mol ⁻¹)	234.099
$\log A$, A (s ⁻¹)	18.023
Contribution	0.113
Step: E→F. Reaction type A3	
Activation energy, E (kJ·mol ⁻¹)	41.943
$\log A$, A (s ⁻¹)	1.018
Contribution	0.228
Step: G→H. Reaction type C1	
Activation energy, E (kJ·mol ⁻¹)	159.674
$\log A$, A (s ⁻¹)	7.209
$\log(\text{AutocatPreExp.})$	1.129
Contribution	0.185
Step: I→J. Reaction type A2	
Activation energy, E (kJ·mol ⁻¹)	77.968
$\log A$, A (s ⁻¹)	7.519
Contribution	0.025

The obtained kinetic parameters are in agreement to the order of magnitudes with E_a s and $\log A$ s estimated by the model-free approach. The results shown in Table 3 do not contain the kinetic parameters with negative values. The actual calculation approach avoids this issue due to the fact that it does not take into account the optimization of the process with the initial parameters from the model-free method, where rather high errors in the kinetic parameter values are obtained. It seems that the coupling of the numerical (model-free) method with a model-based method is the best choice in terms of obtaining reliable kinetic data (therefore, to apply the model-based procedure, the most probable kinetic schemes and corresponding kinetic parameters must be determined by using non-isothermal data and the listed isoconversional methods). Regardless of all the above, an important task is to explain the physicochemical meaning of each of the obtained reaction steps in this complex mechanistic scheme, which describes the thermo-oxidative behavior of the tested resin on a realistic basis. This is shown below.

Reaction Step $I \rightarrow J$ (Temperature Range $\Delta T \sim 130\text{--}245\text{ }^{\circ}\text{C}$)

The single-step reaction $I \rightarrow J$ takes place between $130\text{ }^{\circ}\text{C}$ and $245\text{ }^{\circ}\text{C}$ and at lower degrees of conversion. This step represents the “initial” (inceptive) step in the degradation reaction, related to styrene-divinylbenzene copolymer structure violations. In general, the rigidity degree and the thermal stability of the resin depends on the cross-link agent (divinylbenzene-DVB) amount, present in the polymer structure of the resin [30]. Given that the examined resin represents resin beads in the form of porous micro-spheres with 1% of DVB as the cross-linker [15], actual resin is a more reactive than resin cross-linked with higher amounts of DVB due to the increased number of cross-links [31]. Considering these facts, the cross-linked styrene–DVB polymers have a significant cross-link density and may show a pronounced enhancement in thermal stability and therefore can increase char formation.

The observed part of the process refers to the reaction that takes place at lower temperatures according to the nucleation mechanism, as well as lower values of kinetic parameters (Table 3), which refers to the weakening of unstable reactive sites within the resin polymer support. Namely, the breaking of the C–C bond in the cross-link segment between polymer chains (C—aromatic of the branched chain) is unlikely because this bond is very strong and requires a large amount of energy to break it, even in the presence of oxygen. Consequently, it is most reasonable to assume that weak links are randomly distributed along polymer chains so that oxygen has an effective role in these parts. It can be assumed that oxygen is connected to these weak links. So, oxygen is probably chemically bonded to the polymer chains. Depending on the concentration of oxygen in the reacted system, not all oxygen species lead to chain scission, but probably one part leads to the appearance of thermal chain fission (the scission). Considering the obtained activation energy ($E = 77.968\text{ kJ}\cdot\text{mol}^{-1}$ (Table 3)), a splitting-off of monomer units from chain ends occurs, which requires a much lower activation energy than that for a “harsh” oxidation reaction [32]. The resulted value of E corresponds to the formation of volatile species such as toluene, where the styrene dimer in the presence of a benzyl radical gives toluene and a mid-chain radical (with an activation energy of $\sim 65.9\text{ kJ}\cdot\text{mol}^{-1}$) [33]. Therefore, it can be supposed that single-step reaction $I \rightarrow J$ matches the styrene dimer as the reactant, which produces toluene as the main product, plus the attendance of the mid-chain radical. A corresponding reaction proceeds via the pyrolytic trackway, where resin polymer support is decomposed before the thermo-oxidative process occurs actively. The reaction mechanism proceeds through the two-dimensional nucleation model which is referred to as a gas–solid reaction, with the formation of active nuclei (benzyl radicals). According to reaction type (A2), the reaction takes place with the generation of radicals (nuclei), and a radical generally “grows” two-dimensionally. The reaction rate increases (an accelerated character) with the number of these nuclei (radicals) during the first moments of the reaction or induction period. After this period, the reaction occurs uniformly over the solid surface, and the reaction front advances uniformly to enable the production of aromatic hydrocarbons. Then, this reaction slows down, perfectly matching the transformation pathway with the low energy of the activation. The contribution of this reaction to the entire thermo-oxidative process amounts to $\sim 2.5\%$.

Reaction Step $D \rightarrow E$ (Temperature Range $\Delta T \sim 250\text{--}320\text{ }^{\circ}\text{C}$)

The first reaction step, $D \rightarrow E$, in the sequential stage (Equation (3)) takes place in the temperature range between $250\text{ }^{\circ}\text{C}$ and $320\text{ }^{\circ}\text{C}$ and at the higher conversions. This step proceeds through a diffusion-controlled mechanism (D3 model) with an activation energy of $E = 234.099\text{ kJ}\cdot\text{mol}^{-1}$ (Table 3). Within the considered temperature region, the kinetics of the further degradation of the PS support is controlled by the oxygen diffusion rate through the polymer (in this situation, it should be clearly pointed out that diffusion reactions usually take place with a fairly low activation energy, while in the specific case, the E value is quite high, which means that this reaction is significantly more difficult in terms of the diffusion process and requires a higher expenditure of energy, which is explained later to

be due to the unique behavior of the reaction system). Given the high values of both kinetic parameters, E and $\log A$, the actual reaction step (Table 3) is to some extent “*hindered*”, which depends on the present molecular structures, material morphology, and heating conditions as well. The latter (oxygen diffusion) also affects the degree of mobility of the radicals in the polymer matrix. So, the actual reaction step can be correlated to the radical’s action, involved when oxidation is initiated by external sources, i.e., by thermolysis. The propagation rate is influenced by the mobility of these species. Radicals are formed in pairs and can stay under each other’s influence for a long time and give cage reactions [34]. With this in mind, the rate of the process in this part is most likely regulated by the amount of formed radicals that manage to escape from cages and continue the propagation. Therefore, the actual reaction step can be explained from physicochemical aspects by the following reaction, which is presented by Equation (13):



where $\bullet R_m$ and $\bullet R_n$ are polymer radicals, while brackets “ $< >$ ” designate “*cage*”. This reaction has a diffusion-controlled character. The actual reaction is slow, and the corresponding rate constant is governed by the 3-D translational diffusion of polymer radicals from cages. So, the reaction step $D \rightarrow E$ represents radical–cage diffusion reactions, where radical caged species are reactants (“ D ”), while the escaped radicals (“ E ”) are the intermediate species during the first reaction in the consecutive reaction step. The considered step may occur in the changed viscosity environments, related to the thermally interrupted initial material.

Reaction Step $E \rightarrow F$ (Temperature Range $\Delta T \sim 280\text{--}440\text{ }^\circ\text{C}$)

The reaction step $E \rightarrow F$ occurs in the temperature range between $280\text{ }^\circ\text{C}$ and $440\text{ }^\circ\text{C}$ and represents the second step in the sequential mechanism (Equation (3)). The current step proceeds faster with an accelerating character, where oxygen is taken up and the heating increases, which significantly affects the mobility of ‘free’ radicals. This also affects the higher radical coupling efficiency. Above a temperature of $320\text{ }^\circ\text{C}$, abundant volatile products may be formed, whereby approaching $400/420\text{ }^\circ\text{C}$, a large production of monomers as the main component, with the other volatile products in a smaller amount, can be expected [35]. Namely, the actual step is tightly linked with the previous one, where ‘liberated’ polymer radicals may be involved in the de-propagation pathway [36], producing styrene as the main product, as well as conducting the attack on the PS molecule by intermolecular transfer which leads to the chain scission, giving a product with a shorter polymer chain. The de-propagation reaction as an elementary step in the sequential mechanism is the most probable one, which proceeds with a lower activation energy ($E = 41.943\text{ kJ}\cdot\text{mol}^{-1}$) and with an accelerated character (Table 3). This model corresponds to situations where, above some critical temperature, de-propagation overpowers the propagation and chain growth stops, and the process (growing) then slows down. The contribution of the $E \rightarrow F$ step (~22.8 %) to the overall resin thermo-oxidative degradation process is higher than the contribution of the previous step (Table 3). It should be noted that in accordance with Madras et al. [37], the initiation step can be a controlling step in the pyrolysis process, while for thermolysis, the controlling step is de-propagation or a transfer. Namely, the initiation is the random scission of a bond along the polymer backbone, and it is characterized by a large activation energy, while termination involves the combination of two radicals, leading to small activation energy values. So, the reaction step $D \rightarrow E$, which is characterized by a large activation energy, represents the result of the *cage effect*, where the molecular mobility is reduced, and the radical recombination is more prevalent.

Reaction Step $A \rightarrow B$ (Temperature Range $\Delta T \sim 320\text{--}500\text{ }^\circ\text{C}$)

The actual reaction step occurs in the temperature range between $320\text{ }^\circ\text{C}$ and $500\text{ }^\circ\text{C}$, and it is strictly related to the thermal deconstruction of the Wang linker (Scheme S1, Section S.I., Supplementary Material). So, the considered reaction can be attributed to C–O

homolytic cleavage with the radical's formation, which may instantaneously decompose into gases such as CO and CO₂ [38]. In this case, benzyl alcohol can be formed, and it represents intermediate chemical species for the observed consecutive reaction step (Equation (2)). The process mechanism proceeds through the Fn kinetics model (*n*-th order kinetics) with the activation energy of $E = 289.535 \text{ kJ}\cdot\text{mol}^{-1}$ (Table 3), which belongs to *E* values characteristic for the homolytic cleavage of the C–O bond (251.04 $\text{kJ}\cdot\text{mol}^{-1}$ –292.88 $\text{kJ}\cdot\text{mol}^{-1}$) [39]. The high value of the reaction order amounting to $n = 5.810$ (Table 3) suggests a complex degradation chemistry and the serious thermal “damage” of the resin structure. This obviously leads to the significant increase in the reaction’s complexity through an increase in reaction order (*n*), where radicals are seriously involved in this part of the process. In this moment, the polymer structure is greatly violated by an intensive thermal depolymerization. Therefore, the presented reaction undoubtedly leads to a reduction in the resin molecular structure (a decrease in molecular weight (MW)) by high-temperature implementations. The actual reaction step contributes to the entire thermo-oxidative process, with 20.8% (Table 3).

Reaction Step B→C (Temperature Range ΔT ~ 365–505 °C)

The reaction step B→C (Equation (2)) is attributed to the oxidative degradation of benzyl alcohol, which takes place via the *n*-th order with the *m*-power autocatalysis mechanism (Cnm) (Table 3). Namely, this step proceeds in an autocatalytic manner (with a high *m*-power order by the product) and with a weight factor (autocatalysis factor, K_{cat}) equal to $K_{cat} = 32.211$ ($\sim 0.322 \times 10^2 \text{ s}^{-1}$) (Log(AutocatPreExp.) = 1.508, Table 3). The obtained reaction order of $n \sim 1.764$ suggests that the reaction rate is highest at the beginning but then decreases as the reaction further progresses. With the increase in the temperature and as the reaction progresses, the accumulation of product becomes very large, but the reaction in itself does not rapidly decelerate with the transition of the reactant into the product (a reaction order *n* does not exceed *n* = 2). Since that obtained reaction order is less than 2 ($1 < n < 2$), this means that the *n*-th order reaction model’s function (Supplementary Material, Table S2) decreases more slowly with the conversion than if the reaction order was significantly higher (for example, *n* = 3) (so, the reaction rate decreases much more slowly). Namely, the smaller value of *n* corresponds to the phase boundary reaction of the contracting geometry in heterogeneous material. On the other hand, considering the mathematical form of the kinetic model, Cnm, it encompasses the activation energies of two paths, which are the same regarding *E* (=190.668 $\text{kJ}\cdot\text{mol}^{-1}$, Table 3), where the pre-exponential factors for these paths can be different. The reaction described by the Cnm model involves two competitive pathways. This implies that there is a certain induction period, and after that, the reaction acceleration becomes more significant than the *n*-th order, but it is not as dramatic, as in the case of the pure autocatalysis reaction. The magnitude of this acceleration depends on the values of the “frequency” factors of these two paths (logA and Log(AutocatPreExp.) values in the Table 3) (given that there is a unique value of activation energy, *E*).

The proposed reaction’s mechanism established from the model-based analysis virtually corresponds to the formation of benzaldehyde (C₇H₆O) with H₂O liberation from benzyl alcohol through the *n*-th order pathway and then oxidation of benzaldehyde to benzoic acid (C₇H₆O₂) via the catalytic pathway in the presence of oxygen [40]. It was found [41] that even small amounts of the remaining benzyl alcohol in a system can cause the inhibition of benzaldehyde oxidation. So, the only reaction component which may prevent the further oxidation of benzaldehyde is the remaining benzyl alcohol. This may proceed by quenching the oxidation of benzaldehyde to benzoic acid principally by intercepting acylperoxy radicals, which are responsible for the oxidation of benzaldehyde to benzoic acid [41]. Considering the obtained high value of the pre-exponential factor for the *n*-th order reaction (logA = 13.182, A = $1.521 \times 10^{13} \text{ s}^{-1}$; Table 3), there is a great possibility that at a given temperature and density of molecules, benzyl alcohol reacts with oxygen with an intensive consumption of the reactant. Therefore, it can be assumed that benzyl alcohol does not remain in the degradation process within the reaction system under

observation. Considering the pre-exponential factor obtained for the catalytic pathway ($\sim \times 10^2 \text{ s}^{-1}$), the reaction goes towards the formation of benzoic acid, and it is catalyzed by the presence of benzaldehyde, but the generation of benzoic acid is still lower compared to the yield of benzaldehyde. Consequently, it is reasonable to expect an extremely high yield of benzaldehyde as the main product of the current reaction step and a slightly lower yield of benzoic acid (as the secondary product). Taking this into account, the actual reaction contributes to the entire thermo-oxidative process, with 24.1% (the largest contribution of all individual reactions considered so far).

Reaction Step $g \rightarrow h$ (Temperature Range $\Delta T \sim 510\text{--}620^\circ\text{C}$)

The single-step reaction $G \rightarrow H$ takes place within the temperature range of the thermo-oxidative process, where strong exothermic effects occur at all heating rates (Figure 1b). The actual reaction proceeds with the high conversion values (above $\alpha \sim 0.70$), where isoconversional methods exhibit a negative and then positive E_a values (Figure 3). As can be observed, the model-based approach overcomes the reactionary “pit” identified by the model-free approach, shifting the estimated value of the activation energy ($E = 159.674 \text{ kJ}\cdot\text{mol}^{-1}$, Table 3) across area III[†] right into area IV (Figure 3). This represents an “over-skipping effect”, where the thermo-chemical conversion of the resin enters a phase of the vigorous thermo-oxidative process of the aromatic hydrocarbons as the products are formed from the degradation reactions. Considering these facts, the reaction kinetics of aromatic hydrocarbons largely determine the thermo-oxidative characteristics of the tested resin. Taking into account the reaction kinetics for this part of the process, this should be interesting because the thermo-oxidative properties are guided by a variety of aromatic hydrocarbons that are obtained [42]. In general, the presence of aromatic rings make high sooting tendencies during the thermo-oxidative degradation of the aromatic hydrocarbons. The considered reaction step is described with first-order autocatalysis via the product formed in a complex model (model C1). The actual reaction stage is complex, where many radicals can be involved. However, the main distinction between the first and a higher order of autocatalysis is such that first-order autocatalysis comprises all cases, where a single autocatalytic species is involved on the reactant side. Namely, a “reactant G ” (Equation (10)) is not a single molecule but probably a variety of “molecular building blocks”. Consequently, the single-step mechanism may describe the overall kinetics of the process under the appropriate conditions. The most important phenomenon related to first-order autocatalysis is the fact that when several types of autocatalysts are present simultaneously, all except one are eliminated through the competition of ‘reactants’. Considering the single-step autocatalytic reaction, it increases with time, passes through a maximum value, decreases and finally vanishes.

The simplest explanation of this reaction mechanism and strong exothermicity is the occurrence of a micro-explosion in the hydrocarbons’ thermo-oxidative degradation in a narrow temperature range [43], with the production of CO_2 and H_2O . In this process, the influence of the molecular structure on hydrocarbons’ degradation is essential, especially when hydrocarbon molecules are being attacked by oxygen. In this context, considering all of the above-discussed reaction steps, it can be extracted that there is a reaction step where the resonantly stabilized benzyl radicals have an important role in the formation of aromatic hydrocarbons in the high-temperature zone [44]. Namely, indene (C_9H_8) can be formed through the reaction of benzyl radicals and acetylene [45] (which is created as by-product from the degradation of the resin polymer support [46]), so actually, indene represents the reactant “ G ” in the reaction step $G \rightarrow H$. This reaction represents indene thermo-oxidative degradation, yielding hydro-peroxide in high amounts through first-order autocatalysis. This transformation may lead to the ‘thermal fouling’ in the [4-(hydroxymethyl)phenoxyethyl] polystyrene resin degradation process, which results in an increase in E_a s, considering the isoconversional reaction profile for $\alpha > 0.85$ (Figure 3). Since this reaction takes place in the high-temperature zone and considering the nature of this transformation, the question arises about whether the mass transfer limitations have

an impact in the reaction rate. The oxygen involved in this reaction comes from the vapor phase, and if the reaction proceeds in a liquid phase, then when the rate exceeds the mass transfer capacity, the reaction rate may show the mass transfer limitation. Namely, the mass transfer phenomenon may influence the observed catalytic rate. At the moment, this is difficult to prove because it should be implemented in some kind of chemical reactor with large-scale dimensions (in this case, some tests must be carried out by a reliable method that would measure concentration of dissolved oxygen in the bulk liquid). One might assume that the reaction of interest is extremely fast or instantaneous with respect to the mass transfer, and this fast reaction regime can be attached only to auto-oxidation. This reaction probably includes the reaction of a peroxy radical with an indene molecule in an oxygen-rich environment. Since indene is about three times as reactive as styrene with the addition of the corresponding peroxy radicals [47], for the C1 model, the reaction rate decreases with the consumption of “G”, but once the peroxy radicals are ‘generated’, then they play another role as the “reactants” that boost the progress of the actual reaction. So, the role of peroxy radicals is very important in the thermo-oxidative process of organic molecules regarding indene, which is a typical PAH precursor, which has a special place in its participation of PAHs and soot growth [48].

So, considering the first-order autocatalysis reaction, indene is involved, which, in the presence of the oxygen, produces hydro-peroxides. In addition to these products (organic hydro-peroxides), some others can be expected to be present, such as trimeric and hexameric 2-indanone peroxides [49]. However, there is no evidence for this statement, so this indicates the need for an even deeper analysis with the goal of confirming and identifying chemical species with other analytical instrumental methods as a guide for the next study in the future.

In summary, peroxy radicals ($\text{ROO}\bullet$) may occur as important active intermediates between the indene molecular entity and oxygen, but as product(s), hydro-peroxides (*peroxols*) (and hydroxyl radicals) can be formed, which decompose in high temperatures, with a fierce exothermic heat release. So, because of their inherently high decomposition temperatures and high energy release, it is safe to assume that they are formed in high concentrations, behaving as propellants. Consequently, the considered process stage represents an obvious huge fuel consumption through the fuel oxidation process in the investigated thermo-oxidative degradation process of the tested resin.

A comparison of the hx: model (Equations (2)–(5)) with the experimental ones at various heating rates is shown in Figure 5.

Figure 5 shows that in addition to the high value of R^2 ($R^2 = 0.99955$), the model curves (fits) were not completely lost to the experimental points, as can be seen from Figure 4, in the opposite way, for $T < 420^\circ\text{C}$. However, these curves fit TGA signals in the part of process with a strong exothermic effect much better, unlike the isoconversional methods. Likewise, with regards to the aforementioned part of the degradation process, the fitting power of the model-based method is somewhat weakened (the results would be even better) in the case of the lowest heating rate ($\beta = 5 \text{ K/min}$) (especially at the very end of the process, where the final residual (“plateau”) is established) (Figure 5). Considering this specific stage of the process, in the case of isoconversional methods, a signal distortion occurs, but for the NM method, it is somewhat milder (Figure 4). In the continuation of this analysis, it should be pointed out that the observed discrepancy between the calculated and experimental TGA signals at lower heating rates (the elevated model-computed thermo-analytical signal at lower β s compared to the experimental one) may arise from the change in the local temperature, resulting in a local balance energy exchange, which can also be reflected in the change in the mass of the sample in the corresponding process zones. This could be essential in understanding the influence of the propellant behavior of peroxy radicals in PAH oxidation, reflected by a very strong exothermic effect (see above). The local energy exchange noted above is obviously too fast to be corrected in the fitting procedure by the reaction step in the model (and this is precisely related to the low heating rate, taking into account the characteristics of the system), considering the fixed contribution of each

reaction step to the entire process. The latter is emphasized in the following text (see below). But also, based on the established mechanistic scheme, the reaction mechanism provided is specific for the tested resin in terms of depolymerization, scission, and ultimately cyclisation (char formation). Summarizing all the above-indicated facts, the proposed model scheme (Table S3) quite decently describes the investigated process, especially taking into account the obtained F-test value ($F = 1$).

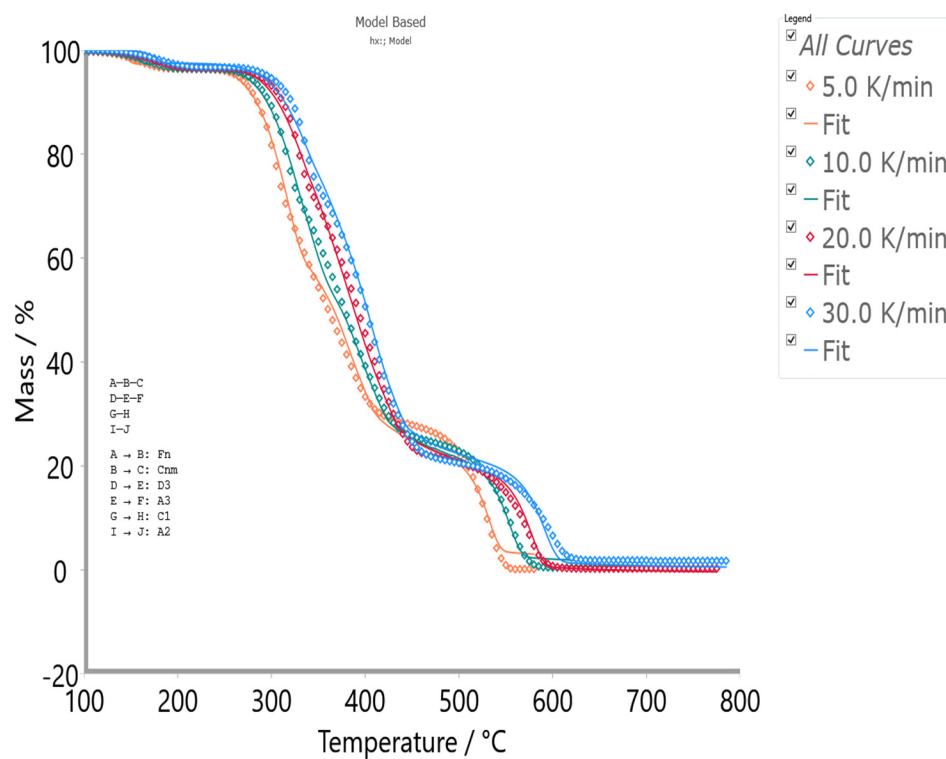


Figure 5. Model-based data fit to the experimental TGA signals at the different heating rates for complex (multi-step) thermo-oxidative degradation of [4-(hydroxymethyl)phenoxy(methyl) polystyrene resin ($R^2 = 0.99955$; all the results of statistical analysis are summarized in Table S3 and the results section in Supplementary Material).

Furthermore, solid- and liquid-phase chemistries can be made intricate by the intertwined transport phenomena, which lead to heat and mass transfer limitations. Consequently, researchers in this case must master the experimental equipment, control the combusted conditions, and provide suitable methods to evaluate thermo-oxidative chemistry. The choice of experimental technique (such as TGA and/or DTA) and the heating program regime (including the magnitude of the heating rates used) represents the most critical decision for the fulfillment of the above-mentioned tasks. Considering these facts, for the applied range of heating rates and the initial experimental conditions, the thermo-oxidative process of such material may consist of various kinetic regimes, from slow to fast. A comprehensive reaction model includes transformations which take place in the “bulk”, with one slow characteristic, and in the liquid–gas phase, with one fast characteristic. Since oxygen represents the active reagent during these transformations, it is “dissolved” in changes that are being made at the gas–liquid interface during thermo-oxidative degradation. Given these characteristics of the process, flow rate parameters can have a strong influence on the kinetics profile of the process itself, especially when it is considered from point of view of the isoconversional principle. Excluding the occurrence of diffusely transmitted effects (diffusivity coefficients), the total mass balance equation must be resolved. Right here, isoconversional methods fail to reach such a quality level of the description of the kinetics of the studied process because they cannot solve the problem with mass balances. But, contrary to this, the model-based method has ‘partial’ success in overcoming

the presented problem because it takes into account in its calculations (from the theoretical approach) the mass transfer parameters, through Equation (12). This is also included in the final mechanistic scheme (with concentration variations with time), which contains all possible kinetic summaries regarding the reaction types present: (i) ‘slow’ kinetics (models D3 and Fn) and (ii) ‘fast’ kinetics (models A2, A3, C1 and Cnm). The latter can be a guide to determine which step represents the process’s rate-controlling step (so, a discussion related to determining which reaction step is the rate-controlling step is given in the Supplementary Material, within Section S.V; see Figures S6 and S7).

However, related to the discussion above, it should be pointed out that despite the large number of reaction models and proposed reaction scheme for the studied process, a perfect fit is not achieved ($R^2 \rightarrow 0.9999$), and some kind of discrepancy is observed for $T > 550$ °C, where the experimental test was carried out at 5 K/min. Namely, it should be clearly pointed out here that the behavior related to the “twist” area (Figure 1d) is also related to the dependence on the thermal history of contribution ($ctb.$ in Equation (12)) of a given reaction step. Because of this, however, the MVNLR approach cannot completely equalize $ctb.$ values in the real time considerations, since it takes a fixed contribution for each reaction step in the fitting procedure cycle. Therefore, this fact affects the reduction in the R^2 , not allowing such an increase in the R^2 value to attain one hundred percent agreement. But, this is not unexpected because there are examples of this behavior, especially in the case of (other) resin thermo-oxidative behavior, that can be observed in the part of the process related to the thermal properties of the aromatics, which cannot easily combust completely in a shorter heating period due to a sudden rise in the temperature [42].

3.4. Adiabatic 24 h Simulations

Theoretical foundations related to the characterization of reactive chemical hazards via the accelerating rate calorimeter (ARC) are presented in the Supplementary Material (Section S.VI.). For a given starting material (resin), the appropriate simulation parameters are selected for different initial temperatures (case 1 and case 2), and both model-free (Friedman) results and model-based (hx:) results are obtained. These data are presented in Table S4 (the results section in the Supplementary Material). For a given set of parameters used in the simulations (Table S4), the corresponding adiabatic $\alpha = \alpha(t)$ (conversion-time) plots for the occurrence of thermal degradation after 24 h, including the Friedman (FR) (model-free) and hx: (model-based) models, are presented in Figure 6a,b (case 1) and Figure 6c,d (case 2). For case 1, which includes a lower initial temperature (≈ 31 °C) and strict adiabatic conditions ($\phi = 1$ (Supplementary Material)), the model-free (FR) results give a simulated plot that deviates upwards from the experimental plot, exhibiting linear TMR extrapolation (for $\alpha \neq 0$) (Figure 6a).

For the conditions listed in Table S4 (case 1) (Supplementary Material), the assumption of a one-step process with simpler kinetics is suggested, where the main equation can be expressed as $c_p \cdot \phi \cdot (dT/dt) = \Delta H \cdot A \cdot f(\alpha) \cdot \exp[-E_\alpha/RT]$ (related to Equation (S17), Supplementary Material) in the absence of a container ($\phi = 1$) and assuming the reaction type expression $f(\alpha) = 1$. Considering parameters c_p and ΔH for the given resin (Table S4), but taking into account the fact that there is no matching between the experimental and simulated plots (Figure 6a), the real situation corresponds to the condition $\phi > 1$, i.e., the thermal inertia increases for an extremely small reached conversion (the influence of the container is higher, and this is a much less representative result of the tested sample itself). In the context of the determination of T_{D24} quantity (Supplementary Material) for the model-free (FR) results in case 1, T_{D24} was found to be 70 °C, which is pretty low. This suggests that for increased thermal inertia, the propagation velocity of the resin flame decreases due to the lower self-heating rate (dT/dt). Considering the results presented in Figure 3, the reaction kinetics evidently are not simple (the assumption attached to $f(\alpha) = 1$ in the above expression fails), while the main equation was governed by the term $\exp[-E_\alpha/RT]$, where $E_\alpha \neq const$. So, for case 1, the model-free (FR) model (Figure 6a) more closely matches the measurements in the presence of a container ($\phi > 1$), where all

heat released is not used to heat the sample only and there is an energy dissipation. This suggests that the TMR is achieved at a very low conversion (almost when the reaction has not even started), producing low T_{D24} with the low value of the initial temperature. This leads to controversy regarding the calculation of the maximum temperature of the synthesis reaction (MTSR), which, in this case, is still undetermined (the thermal accumulation of the reagent is not defined). Since the model depends on E_α , A and $f(\alpha)$, the problem with the inaccuracy of the model-free results in the simulation tests lies in not recognizing the exact kinetic mechanism (not knowing the exact form of the $f(\alpha)$ function) of the considered transformation, then introducing larger errors in the kinetic parameters, both E_α and A (see Figure 3, Figures S2 and S3), as well as drawbacks related to issues that were described previously. So, the results obtained by the model-free approach in case 1, strongly deviate from the strict adiabatic conditions and do not correspond to the given conditions of the thermal safety tests. Considering the low initial temperature (case 1), the calorimeter test starts for the sample not totally degraded (Figure 6a), while simulated test starts as if a certain degradation has already occurred, which is very difficult to achieve from an experimental point of view, given condition $\phi = 1$. Consequently, this situation corresponds to the state of the corrected ϕ factor, which is not equal to unity. Correcting the ϕ factor can be inaccurate, since the model-free approach does not take into account changing the analytical form of the reaction model and maybe the gas evolution during the reaction, both of which affect the ϕ factor during the reaction. Furthermore, the next factor is that the current method assumes a single reaction occurs, whereas a complex mixture of reactions may in fact take place. Likewise, the accuracy of the data obtained is also a factor in the assessment of the reliability of the behavior of runaway reactions. So, the simulation performed under case 1 with the model-free data corresponds to a very low adiabatic environment. On the other hand, the same kinetic data extracted from the model-free method for case 2 (when there is a significant increase in the initial temperature, $=91^\circ\text{C}$ (Figure 6c)) lead to a near match between the experimental and simulated plots approaching condition $\phi = 1$ (a strict adiabatic environment in the absence of the container). Both plots approximately start for the undegraded sample ($\alpha(t) \approx 0$), exhibiting further an expanded range of conversion values up to $\alpha \approx 0.01$ with a temperature declination of $+0.25^\circ\text{C}$ (Figure 6c). In this case, the value of $T_{D24} = 145^\circ\text{C}$ was found, which, for 75°C , is higher than the T_{D24} value obtained for case 1. However, these conditions correspond more to the real situation for the obtained kinetic parameters from the model-free method. In this case, the primary reactions are probably taking place and represent desirable reactions, while the vigorous exothermic secondary reactions (undesirable) are excluded, and there is no danger of the runaway reactions. To justify this fact, the maximum temperature of synthesis reaction is calculated which amounts to an $\text{MTSR} = 134.4^\circ\text{C}$, and this value is lower than T_{D24} ($=145^\circ\text{C}$), confirming that after finishing a primary reaction, the rapid secondary reaction does not occur, and therefore, the risk of a runaway reaction is very low. Considering the main equation presented above, the dimensionless form of the activation energy is $\zeta = E_\alpha / RT$, so generally, the ζ of the slow reactions is higher than that of the fast reactions. Consequently, the reaction rates with a high activation energy are more sensitive to the temperature, with respect to the reaction rates with a low activation energy. In this context, the maximum accumulation of the reagents of high activation energy reactions is lower than that of relatively smaller activation energy reactions in the higher initial temperatures, while an approximately inverse relationship can be presented in the lower initial temperature. This is the one of the main reasons for the difference between the results presented in the above discussion and the observations in Figure 6a,c.

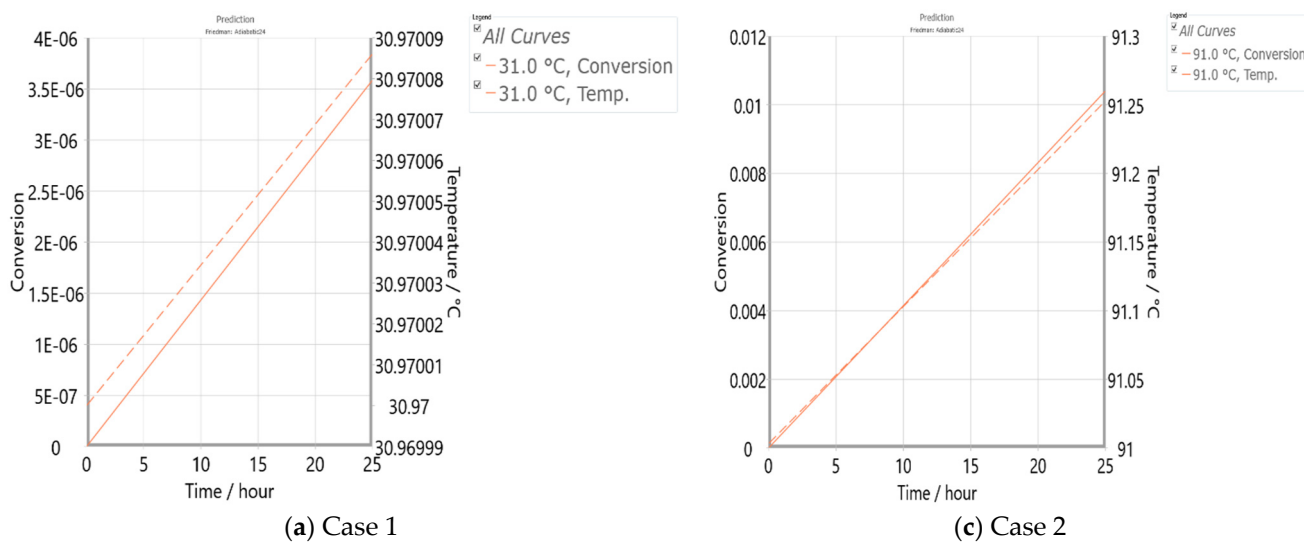


Figure 6. $\alpha = \alpha(t)$ adiabatic conversion curves for [4-(hydroxymethyl)phenoxyethyl] polystyrene resin thermo-oxidative degradation process after 24 h, obtained for case 1 (Table S4), according to Friedman (FR) (model-free) (a) and the hx: (model-based) (b) models, and for case 2 (Table S4), according to Friedman (FR) (model-free) (c) and the hx: (model-based) (d) models (*solid colored line*—calorimeter measurement/experimental signal; *dash colored line*—the simulated signal to time to maximum reaction rate, e.g., 24 h).

Considering case 1 for the model-based results (for the proposed mechanistic scheme hx,:.) (Figure 6b), there is a complete change in the form of $\alpha(t)$ plots, where both curves (measured and simulated) receive an acceleratory character. There is a minor upward deviation (compared to Figure 6a) of the simulated curve from the experimental curve. In the actual case, regarding the achieved small conversion value at 24 h, the value of $T_{D24} = 85^\circ\text{C}$ is obtained. Actually, the calculated MTSR significantly surpasses T_{D24} ($\text{MTSR} = 250.3^\circ\text{C}$), revealing the presence of a secondary process with self-heating (in a spontaneous manner). For the observed case (case 1 in Table S4 for the model-based results), the ζ values are above 30 ($\zeta > 30$), indicating the presence of reactions with a high activation energy that tend to change the $\alpha(t)$ plot in an acceleratory shape. The model-based method highlights reactions with an accelerating degree such as those that proceed with high E values (reaction steps B→C and G→H (Table 3)), with autocatalytic behavior. So, in this situation, the model-based results emphasize the presence of fast oxidation reactions, revealing that for the low initial temperature, MTSR rises above T_{D24} , significantly changing the form of the conversion pathway from those presented in Figure 6a. Considering the results in Figure 6b and those presented in Figure 6a regarding to simulation tests, it follows that even a very small non-zero conversion strongly affects the reaction and the kinetics estimated under the “zero” assumption ($\alpha = 0$), and this can be unsafe or even completely wrong. Therefore, the calculations performed by the model-based approach seem to give true values of the kinetic quantities in comparison with the ones shown for case 1 in Figure 6a. The latter retracts the identified shortcomings in the implementation of model-free methods for the investigated process (see earlier discussions). However, interesting results are obtained for case 2, when there is an increase in the initial temperature (Table S4), observing the results obtained from the application of the model-based approach (Figure 6d). Upon increasing the initial temperature, both plots change forms from an acceleratory (Figure 6b) to the deceleratory character (Figure 6d), where they coincide up to 2.2 h ($\phi = 1$) (also, there is a small accelerating segment at the very beginning, which takes about 0.20 h (12 min.; $\alpha \approx 0.1\%$)). After 2.2 h, there is an upward deviation of the simulated plot from the measured one ($\phi > 1$), where a uniform deviation is noted in the saturation section above 4 h (Figure 6d). Under the given conditions (case 2), the form of

the $\alpha(t)$ plot corresponds to the dominance of reactions with retarding characteristics, such as the diffusion-controlled mechanism (reaction step $D \rightarrow E$ (see above discussion)). For the observed case, the value of $T_{D24} = 175^\circ\text{C}$ is obtained, while the maximum temperature of the synthesis reaction amounts to an MTSR = 114.7°C . The obtained results suggest that rapid reactions are not initialized, and there is no risk of uncontrolled reactions. In this observation, based on the results presented in Figure 6d, up to approximately 2.2 h, the reaction system obeys the strict adiabatic conditions (where all the heat released is used to heat the tested sample) which includes a lower activation energy and may trigger the high heat release rate, which in turn results in a lower TMR value (Supplementary Material) than the real adiabatic value. At a high constant temperature, a higher activation energy can be involved, where ζ values are below 30 ($\zeta < 30$), but for the higher initial temperature, it causes a change in the ϕ factor to $\phi > 1$ (Figure 6d). The higher the ϕ , the slower the heat release rate of the sample in the initial stage, the lower the temperature rise rate and the longer the time taken to reach the TMR.

So, considering the simulations related to the model-based results, there are obviously two scenarios: (1) Temp. initial \downarrow , MTSR $> T_{D24}$, $\phi > 1$, $E \uparrow$, $\zeta > 30$: acceleratory–autocatalytic behavior, and (2) Temp. initial \uparrow , MTSR $< T_{D24}$, deceleratory behavior, where a) $\phi = 1$ for $E \downarrow$, $\zeta \approx 20$, and b) $\phi > 1$, $E \uparrow$, $20 < \zeta < 30$. Based on these scenarios derived from the model-based data in adiabatic 24 h simulations, there is a clear difference from the model-free results, which deviate from realistic assessments of the thermal risks and hazards. The model-based data established in this work provide more accurate kinetic quantities for this type of analysis, necessary for their application in batch reactors. For the observed cases considered through the established scenarios, the decisive factor is the initial temperature (Table S4), which is associated with the achieved time to maximum rates (TMRs), where the safety of industrial processes depends on it (which is an important to predict condition for the safe storage of chemicals, such as the resin investigated in this study, via the above experiments).

Adiabatic Simulations from Model-Based Results and Influence of Heat and Mass Transfer Limitations

The self-heating scenario which was determined by previous analyzes (scenario 1) corresponds to case 1 in Figure 6b. For the actual case scenario, there is an increase in ϕ with higher E values, when the experiments take place using an ARC. This is mainly because the calculated kinetic parameters obtained by the ARC data depend on the adiabatic temperature rise rate of Equation (S17) (Supplementary Material). With the influence of larger ϕ values, the measured adiabatic temperature rise curve of the sample is not the degradation curve of itself, and it is the curve which is formed after a sample's "passivation". It should be noted that the performed analysis of the kinetic parameters is not incidental to resin degradation but to the degradation of the "complex sample" that includes the resin spherical particle, the heat and mass transfers, as well as heat transfer information, as comprehensive parameters. In safety terms, $\phi \approx 1$ holds for an increasing dosage of the sample, and the refined ideal adiabatic data are more reliable, and contrarily, $\phi > 1$ holds for a decreasing dosage of the sample. Based on the above scenarios (1) and (2) (see above), the different conditions for ϕ that have been found indicate that the process follows different mechanisms. Of course, the latter can be influenced by the phenomena related to heat and mass transfers.

There are several dimensionless numbers which have been developed for examining the heat transfer in the thermo-chemical conversion process of a single particle of the material. These numbers are the Biot number (Bi) (which compares external and internal heat transfer rates), pyrolysis number-1 (P_{y1}) (which compares the internal heat transfer rate and the reaction rate) and pyrolysis number-2 (P_{y2}) (which compares external heat transfer with the reaction rate) [50]. Pyle and Zaror [51] provide a paper that describes various regimes in which one phenomenon controls the effective rate of the thermo-chemical transformation of the investigated material in the chemical reactor. If the particle is large

enough that Bi is greater than $Bi = 10$ and P_{y1} is less than 1, the heating is limited by internal thermal conduction. Consequently, the heating rate of the reactor in some respects is less important than the particle size.

Table 4 lists the obtained values of Bi , P_{y1} and P_{y2} for the single particle of the tested resin ([4-(hydroxymethyl)phenoxyethyl] polystyrene resin (Scheme S1)) and the corresponding regions of validity for the existing models under micro-reactor conditions [50].

Table 4. The Bi , P_{y1} and P_{y2} values obtained for tested resin single particle, correlated to the regions of validity for a single-particle model [50].

Model	Approximate Range of Validity			Tested Resin Model *		
	Bi	P_{y1}	P_{y2}	Bi	P_{y1}^{**}	P_{y2}
I: Non-controlled conditions	All	All	All			
II: External heat transfer-controlled	<1	>1	>1	0.000315	440.917	0.139
III: Kinetics-controlled	<1	>10	>10			
IV: Internal heat transfer-controlled	>50	<10 ⁻³	<<1			

* Resin physical properties: R (resin particle size) = 0.045 mm; λ (thermal conductivity) = 0.10 W·m⁻¹·K⁻¹; h (the external heat transfer coefficient) = 0.70 W·m⁻²·K⁻¹; ρ (bulk particle density) = 1.12 g·cm⁻³; k (apparent reaction rate constant) = 0.02 s⁻¹. ** The large P_{y1} value indicates that internal transfer limitations are not impediments to degradation reactions.

For the resin particle size of 0.045 mm (a smaller particle; < 1 mm), the Biot number (Bi) has less than unity (<1) (Table 4). This is indicated during the external heat transfer-controlled process. In accordance with Pyle and Zaror [51], for the large value of P_{y1} (Table 4), the real model for the tested resin particle can be considered as a conjunction between the Bi and P_{y2} values. Namely, our case fits $Bi \ll 1$ and $P_{y2} \ll 1$ (Table 4), where the kinetics are so fast that the carbonization is uniform throughout the particle, and external heat transfer controls the overall rate. These results do not match the “pure” kinetic control regime but the approach of the kinetically controlled, carried out in an increasing manner by decreasing the temperature and particle size (decreasing Bi and increasing P_{y1} (Table 4)). Considering our experimental conditions which are conducted in this work, the heating rate (as mentioned previously) represents a critical factor which defines the conditions necessary for the thermally efficient degradation of the studied resin in an air atmosphere. Namely, in the current experiments, the resin particle (with its spherical shape) was heated under the linear heating program, which is represented mathematically as $T = T_0 + \beta \cdot t$, where T_0 , β and t are the particle’s initial temperature, the heating rate and time, respectively. This represents a simplification used for a “lumped” heat transfer, wherein the spatial temperature gradients are neglected. So, the actual approximation is applicable for reaction systems whose Biot number (Bi) is less than or equal to 0.10 (Table 4). This corresponds to certain convenient experimental conditions such as those in thermogravimetric analysis (TGA) and to a process which is subjected to kinetic control conditions, using small particle sizes. Thus, if this condition is met, and there are not convective heat transfer limitations, then reaction rate constants can be considered as “intrinsic” [50,51], which means that the transport phenomena are lumped with chemical reaction rates. It should be emphasized here that it is a difficult to compare experimental results obtained for global-scale yields to the kinetic parameters obtained in this paper based on micro-scale yields. These should be considered as simulation tests that would be useful for serious considerations of the results in the reactors of wider application. For an intrinsic kinetic study, the most commonly used devices are some kind of free-fall reactor and reactors coupled with MS (mass spectrometry) monitoring, which minimize the heat transfer limitations and secondary gas-phase reactions. Summarizing the presented results (Table 4), they do not fit the conditions for the “thermal wave” or the internal heat

transfer control, which was obviously not achieved in this work. Therefore, this discussion is executed from the perspective of analytical solutions and scaling analysis.

Using the simulation test results discussed in the previous section, the value of internal heat source per volume (Q) ($\text{W}\cdot\text{cm}^{-3}$) is established through the formula $Q = \rho_p \cdot v_p \cdot \Delta H \cdot (\text{d}\alpha/\text{dt})$, where ρ_p is the bulk particle density ($=1.12 \text{ g}\cdot\text{cm}^{-3}$), v_p is the resin volume fraction, excluding DVB presence ($=0.855 [-]$), ΔH is the enthalpy ($=120 \text{ J}\cdot\text{g}^{-1}$) and $\text{d}\alpha/\text{dt}$ is the reaction rate (s^{-1}), which depends on the resin degradation kinetics. The reaction rate was calculated for the kinetic parameters of the reaction with the autocatalytic behavior (Cnm model) that exhibited $\zeta > 30$. The obtained value of Q amounted to $Q = 0.115 \text{ W}\cdot\text{cm}^{-3}$ (either $Q = 115,000 \text{ W}\cdot\text{m}^{-3}$). On the other hand, for the diffusion reaction (D3 model) with deceleratory kinetics behavior, the Q value was calculated, including the reaction rate which was obtained for the kinetic parameters of that reaction, exhibiting $\zeta < 30$. In this case, the obtained value of Q amounted to exactly $Q = 0.230 \text{ W}\cdot\text{cm}^{-3}$ (either $Q = 230,000 \text{ W}\cdot\text{m}^{-3}$). For the last one, more heat had already been generated, considering the volumetric heat source values (the both values). This was a direct energy connection between the influence of the kinetic parameters and the different reaction mechanisms. Also, this was linked with different conditions for the ϕ factor (considered in the previous section) (see the proposed scenarios; Figure 6b,d) which were driven by different reaction models, thus describing the main mechanistic key points of the investigated thermo-oxidative degradation process (see also Section S.V. in the Supplementary Material).

Considering the discussion about the influence of mass transfer limitations on the catalytic reaction rate (see above), certain considerations are limited because the mass transfer coefficient determination should carry out on the applied chemical reactor(s), which is not used in this study. Therefore, taking the reactor's conditions, the mass transfer is defined as the net movement of one species, e.g., one of the reactants, from one point to another within the reactor due to diffusion and/or convection. This is especially crucial in the case of multi-phase reactions, e.g., gas–liquid reactions, where one of the reagents needs to migrate by diffusion from one phase to another. Given the limitations, this should be viewed in this study purely phenomenologically. In addition, the rapid release of gaseous products may generate significant pressure within the resin particles because volatiles cannot be instantly evacuated. This may cause internal resin structure cracks, leading to an increase in the quantity of micro-pores. By passing the reactionary system through a molten phase, the internal structure can warp and block the pores at higher heating rates. So, considering the fast autocatalytic moment of the considered process, related to indene auto-oxidation with a high accumulation of hydro-peroxides, for this reaction environment, the concentration of the reactant in the bulk of fluid media is an important quantity. So, the temperature, partial pressure, the extent of oxygen dissolution, the equivalence ratio (Φ) of indene/air and indene concentration can affect the time to indene “ignition” [52]. Namely, in order to obtain the rate of the reaction that leads to the degradation of indene in the presence of oxygen in the reactor conditions, all the above-mentioned quantities should be taken into account and inserted into some form of newly constructed equation of the Arrhenius type. On the other hand, for the calculation of mass transfer limitations of a gas-phase reaction inside the chemical reactor (for example, in a fixed bed reactor), a large number of variables needs to be considered in the simulation tests, as can be seen in the paper of García-Sánchez et al. [53]. Therefore, after finding the optimal reaction rate for the indene catalytic reaction under chemical reactor conditions, it should then be compared with the observed reaction rate, which may be affected by the external mass diffusion [54] and intrinsic reaction rate of the catalyst species. If a detailed analysis indicates the authors' assumptions presented in “Reaction Step g→h (Temperature Range $\Delta T \sim 510\text{--}620^\circ\text{C}$ ”), only then can it be confirmed that the reaction rate can shows the mass transfer limitation. Consequently, this study is limited by the above-mentioned tests, but it provides the basis for future work that can simulate the thermo-oxidative degradation of the considered resin under real reactor conditions. Finally, with the above information entered, it is possible to determine the service life of the studied resin in large-scale applications. Based on the

calculated parameters, thermal degradation can have a strong impact on the establishment of conditions in the appropriate types of reactors. Therefore, some longstanding questions that exist in the study of resin thermo-oxidative degradation can be addressed with this work.

4. Conclusions

In this paper, a detailed analysis of the possibilities and limitations of model-free and model-based kinetic approaches in the detection and identification of the complex reactions that take place during thermo-oxidative degradation was implemented. As a test system for the implemented analysis, [4-(hydroxymethyl)phenoxyethyl] polystyrene resin (*p*-alkoxybenzyl alcohol resin) was analyzed. In the case of isoconversional analysis, Friedman (FR), Vyazovkin (VY), and numerical (NM) isoconversional (model-free) methods were used. The results that were obtained using the model-free approach were compared to those obtained via the model-based approach (using the multivariate non-linear regression (MVNLR) calculation procedure). The advantages and disadvantages of these approaches applied to the thermos-oxidative degradation process of the tested resin were highlighted and analyzed. The model-free methods provide an accurate number of process stages that occurred during the process, which, on the basis of $E_a = E_a(\text{conversion})$ profiles, determined the possible occurrence of corresponding types of reactions and identified negative reaction rate dependence on the temperature. This behavior was expressed as barrierless reaction step or where the thermo-oxidative reaction proceeded spontaneously. It was shown that this phenomenon was closely related to strong exothermicity. The last thermo-oxidative process stage was linked to the oxidation reactions of hydrocarbons obtained from the degradation reactions of both the polymer structure of the resin and the Wang linker structure (benzyl alcohol moiety thermal deconstruction). Limitations of the model-free methods in reconstructing a kinetic complexity were related to the appearance of parallel reactions, which were not able to provide an answer regarding which types of parallel reactions dominated. This refers to whether some of them were consecutive or single-step reactions. Likewise, on the basis of this analysis, it could not be established whether there was a presence of acceleratory reactions, as well as their number. Isoconversional kinetic methods could not overcome the problem that arose due to the mass transfer limitations during the thermo-oxidative degradation of carbon materials.

On the other hand, the application of the model-based method gives much better results compared to previous one, regarding the description of complex thermo-oxidative mechanisms. The model-based method overcomes more successfully the problem associated with mass transfer because its calculation machinery has capabilities to provide the correct solution of the total mass balance equation. But, despite this, a perfect fit with the experimental data is not achieved due to the dependence on the thermal history of contribution of a given (considered) reaction step. So, the MVNLR cannot completely equalize the contribution values in real-time data analysis since it takes into account the fixed contribution for each reaction step in the fitting procedure cycle. However, the current method allows the estimation of the rate-controlling steps in thermo-oxidative processes, regarding the influence of the heating rate (β). It is found that the key mechanism is an autocatalytic formation of benzaldehyde from the benzyl alcohol moiety of the Wang linker and oxidation of benzaldehyde to benzoic acid, proceeding as two parallel reactions. Namely, it is established that benzaldehyde is strongly favored in this rate-determining step compared to benzoic acid. Also, it is showed that the transport phenomenon may be also the rate-determining step (in the set of “intrinsic” kinetic parameters). However, for this transformation, it is concluded that the applied heating rate has a crucial role. For a consecutive reaction mechanism, the low heating rate favors the participation of the cage radicals, which generates gaseous products, with the exclusion of the de-propagation reaction (as an intermediate step), making the mechanism proceed as a single-step reaction. At a high heating rate, the de-propagation reaction cannot be ignored in the analyzed case, so this additional step complicates the process to a significant extent, which is not

desirable from practical interests. Considering both cases, the use of lower heating rates is strongly recommended ($\beta \leq 10 \text{ K/min}$), which is also confirmed based on the behavior of thermo-oxidative degradation characteristic indices. One of important advantages of model-based computation is the ability to recognize a reaction step with extremely fast production, which leads to a fierce exothermic heat release.

In the continuation of this study, it is found on the basis of the adiabatic 24 h simulation tests that there are two scenarios of the thermal history of the examined reaction system under the given conditions, considering model-based data. One contains inequalities of the type $\text{MTSR} > T_{D24}$ and $\phi > 1$, including the dominance of the reaction with acceleratory (autocatalytic) behavior with a high activation energy, and another containing an inequality of the type $\text{MTSR} < T_{D24}$, which includes the reaction with deceleratory behavior, which has two subcategories. These subcategories are characterized by states of the reaction system, with the variable behavior of the ϕ factor and different activation energies. In the current analysis, it is found that initial temperatures represent a decisive parameter, which is associated with the achieved time to maximum rates (TMRs), which is important for the assessment of thermal risks in chemical processes.

It is also concluded that external heat transfer controls the overall rate, where the “pure” kinetic control regime has not been reached but is approached when lowering the temperature and the size of the resin particles. Regarding the latter, only phenomenological questions can be taken into account and answers be obtained accordingly. However, for a wider inspection of these phenomena, the research must be expanded with much more complex simulations, related to the reactions that would take place in chemical reactors, for the thermo-chemical conversion of this resin into valuable products.

The study of complex processes generally requires the understanding of more basic or fundamental events. So, future examinations of the pretreatment of “spent” resin should start with an analysis of unused resin on a small-scale, related to commercial thermal analysis experiments, via oxidative pyrolysis (i.e., the oxidative degradation thermally induced in air). Of prime importance regarding the results in this study (mechanistic models which were developed here and demonstrated very good predictive abilities for the investigated process of the tested polymer-based material) is that they can be possibly realized in small-sized reactor facilities (the propelling reaction nature of the resin allows it to be fed into the incinerator/reactor under its own pressure, avoiding the need for injection pumps).

Supplementary Materials: The following supporting information can be downloaded at: <https://www.mdpi.com/article/10.3390/fire7050165/s1>, S.I. Chemical composition and properties of the resin used in the study, S.II. Characteristic process indices, S.III. Kinetic analysis, S.III.1. Model-free analysis: Friedman (FR), Vyazovkin (VY) and numerical (NM) methods, S.III.2. Model-based analysis, S.IV. Preliminary determination of the type of reaction models involved in the resin degradation mechanism (related to additional discussion), S.V. Kinetic analysis related to the determination of the rate-controlling steps in the resin degradation process (related to additional discussion), S.VI. Safety analysis-characterization of runaway reactions and use of kinetic data in adiabatic simulations (adiabatic 24 h prediction) [55–81]. References: Figure S1: Thermal stability results related to [4-(hydroxymethyl)phenoxyethyl] polystyrene resin thermo-oxidative degradation process: (a) fitting applied to evolution of T_i values with β 's, (b) fitting applied to evolution of T_p values with β 's and (c) fittings applied to possible evaluations of T_b values with β s. For each observed case, appropriate rational power relationship (a) and b) and exponential relationship, with additional linear relationship (c), were shown on the same graph (the corresponding values of parameters of the fitting are also indicated) [the dashed line under the case c) shows ‘irregular’ trend of experimental points]; Figure S2: Multiconversional dependent logarithm of pre-exponential factors ($\log A(\alpha)$) obtained by Friedman (FR), Vyazovkin (VY) and numerical (NM) methods, for thermo-oxidative degradation process of [4-(hydroxymethyl)phenoxyethyl] polystyrene resin (Scheme S1); Figure S3: The deviation (ε_m) in the percentages of E_a values of FR, VY and NM methods from their mean E_a values (FR: $E_{a(\text{mean})} = 142.498 \text{ kJ}\cdot\text{mol}^{-1}$; VY: $E_{a(\text{mean})} = 140.682 \text{ kJ}\cdot\text{mol}^{-1}$; NM: $E_{a(\text{mean})} = 143.023 \text{ kJ}\cdot\text{mol}^{-1}$) for thermo-oxidative degradation process of [4-(hydroxymethyl)phenoxyethyl] polystyrene resin;

Figure S4: Friedman's (FR) isoconversional plots at every considered conversion value (with a step of $\Delta\alpha = 0.01$; an increase in the conversion (conversion is designated by "x" according to Kinetics Neo operational tool sheets, where $x \equiv \alpha$) goes from right to left), constructed for thermo-oxidative degradation process of [4-(hydroxymethyl)phenoxyethyl] polystyrene resin at four different heating rates, $\beta = 5, 10, 20$ and 30 K/min (orange \diamond : 5 K/min , dark green \diamond : 10 K/min , crimson red \diamond : 20 K/min and light blue \diamond : 30 K/min); Figure S5: Friedman's (FR) isoconversional plots at the selected conversion values ($x \equiv \alpha = 0.02, 0.05, 0.1, 0.2, 0.3, 0.4, 0.5, 0.6, 0.7, 0.8, 0.9, 0.95$ and 0.98) (conversion is designated by "x" according to Kinetics Neo operational tool sheets, where $x \equiv \alpha$), for thermo-oxidative degradation process of [4-(hydroxymethyl)phenoxyethyl] polystyrene resin at four different heating rates; Figure S6: Rate constant's behavior with the temperature, according to $k_{step}(T) = A_{step} \cdot \exp(-E_{step}/RT_{(range)})$: (a) for I-J, D-E, E-F, and A-B steps (5 K/min), (b) for B-C step (n -th order and m -autocatalytic shares) and G-H step (for the first-order with autocatalysis share) (5 K/min), (c) for I-J, D-E, E-F, and A-B steps (30 K/min) and d) for B-C step (n -th order and m -autocatalytic shares) and G-H step (for the first-order with autocatalysis share) (30 K/min); Figure S7: Mean rate constants for each individual reaction step in hx:, model, for a) $\beta = 5 \text{ K/min}$ and b) $\beta = 30 \text{ K/min}$; Scheme S1: The concept of the solid support with linker/spacer, which together form [4-(hydroxymethyl)phenoxyethyl] polystyrene resin (solid colored ball represents polystyrene (PS) solid support); Table S1: Characteristics of [4-(hydroxymethyl)phenoxyethyl]polystyrene (4-benzyloxybenzyl alcohol) resin beads; Table S2: Reaction models used for solid-state kinetics evaluations studied in this work, within Kinetics Neo 2.6.6.7 software. The rate expression: $de/dt = k(T) \cdot f(e,p)$, ($k(T)$: Arrhenius-type temperature-dependent rate constant, $f(e,p)$: the reaction model; e -the starting concentration of the reactant ($e = 1 - \alpha$), p -the concentration of the final product ($p = \alpha$ (conversion)) [within the theoretical part]; Table S3: Statistical analysis results (a statistical fit quality) for proposed hx:, model (obtained from model-based method) in the case of [4-(hydroxymethyl)phenoxyethyl] polystyrene resin degradation; Table S4: Conditions for adiabatic 24 (h) predictions using Friedman (FR) (model-free) and hx:, (model-based) models in terms of thermal safety of [4-(hydroxymethyl)phenoxyethyl] polystyrene resin.

Author Contributions: Conceptualization, methodology, software, validation, formal analysis, data curation, writing—original draft, writing—review and editing, visualization, supervision, project administration, funding acquisition, B.J.; methodology, validation, formal analysis, investigation, data curation, writing—review and editing, supervision, V.D.; methodology, validation, formal analysis, data curation, writing—review and editing, supervision, F.V.; methodology, validation, formal analysis, resources, data curation, writing—review and editing, supervision, M.J.; methodology, software, validation, formal analysis, investigation, data curation, writing—review and editing, supervision, N.M. All authors have read and agreed to the published version of the manuscript.

Funding: This research was funded by the Ministry of Science, Technological Development and Innovation of the Republic of Serbia under contract numbers 451-03-66/2024-03/200017 ("Vinča" Institute of Nuclear Sciences, the National Institute of the Republic of Serbia) and 451-03-65/2024-03/200105 (the Faculty of Mechanical Engineering).

Institutional Review Board Statement: Not applicable.

Informed Consent Statement: Not applicable.

Data Availability Statement: Data are available on request from the authors.

Acknowledgments: The authors would like to thank a regular member of the Serbian Academy of Sciences and Arts (SANU), Slavko Mentus, for their useful suggestions and comments related to this study.

Conflicts of Interest: The authors declare no conflicts of interest.

References

1. Brown, M.E.; Maciejewski, M.; Vyazovkin, S.; Nomen, R.; Sempere, J.; Burnham, A.; Opfermann, J.; Strey, R.; Anderson, H.; Kemmler, A.; et al. Computational aspects of kinetic analysis. Part A: The ICTAC Kinetics Project: Data, methods and results. *Thermochim. Acta* **2000**, *355*, 125–143. [[CrossRef](#)]
2. Vyazovkin, S.; Sbirrazzuoli, N. Isoconversional kinetic analysis of thermally stimulated processes in polymers. *Macromol. Rapid Commun.* **2006**, *27*, 1515–1532. [[CrossRef](#)]

3. Burnham, A.K.; Dinh, L.N. A comparison of isoconversional and model-fitting approaches to kinetic parameter estimation and application predictions. *J. Therm. Anal. Calorim.* **2007**, *89*, 479–490. [[CrossRef](#)]
4. Vyazovkin, S. Some confusion concerning integral isoconversional methods that may result from the paper by Budrigeac and Segal “Some methodological problems concerning nonisothermal kinetic analysis of heterogeneous solid-gas reactions”. *Int. J. Chem. Kinet.* **2002**, *34*, 418–420. [[CrossRef](#)]
5. Vyazovkin, S.V.; Lesnikovich, A.I. An approach to the solution of the inverse kinetic problem in the case of complex processes. Part 1. Methods employing a series of thermoanalytical curves. *Thermochim. Acta* **1990**, *165*, 273–280. [[CrossRef](#)]
6. Maciejewski, M. Computational aspects of kinetic analysis. Part B: The ICTAC Kinetics Project: The decomposition kinetics of calcium carbonate revisited, or some tips on survival in the kinetic minefield. *Thermochim. Acta* **2000**, *355*, 145–154. [[CrossRef](#)]
7. Vyazovkin, S.; Chrissafis, K.; Di Lorenzo, M.L.; Koga, N.; Pijolat, M.; Roduit, B.; Sbirrazzuoli, N.; Suñol, J.J. ICTAC Kinetics Committee recommendations for collecting experimental thermal analysis data for kinetic computations. *Thermochim. Acta* **2014**, *590*, 1–23. [[CrossRef](#)]
8. Koga, N.; Vyazovkin, S.; Burnham, A.K.; Favergon, L.; Muravyev, N.V.; Pérez-Maqueda, L.A.; Saggese, C.; Sánchez-Jiménez, P.E. ICTAC Kinetics Committee recommendations for analysis of thermal decomposition kinetics. *Thermochim. Acta* **2023**, *719*, 179384. [[CrossRef](#)]
9. Vyazovkin, S.; Burnham, A.K.; Favergon, L.; Koga, N.; Moukhina, E.; Pérez-Maqueda, L.A.; Sbirrazzuoli, N. ICTAC Kinetics Committee recommendations for analysis of multi-step kinetics. *Thermochim. Acta* **2020**, *689*, 178597. [[CrossRef](#)]
10. Moukhina, E. Determination of kinetic mechanisms for reactions measured with thermoanalytical instruments. *J. Therm. Anal. Calorim.* **2012**, *109*, 1203–1214. [[CrossRef](#)]
11. Friedman, H.L. Kinetics of thermal degradation of char-forming plastics from thermogravimetry. Application to a phenolic plastic. *J. Polym. Sci. Part C Polym. Symp.* **1964**, *6*, 183–195. [[CrossRef](#)]
12. Vyazovkin, S. *Isoconversional Kinetics of Thermally Stimulated Processes*, 1st ed.; Springer: London, UK, 2015; pp. 1–59.
13. Wilkie, C.A.; Morgan, A.B.; Nelson, G.R. *Fire and Polymers V. Materials and Concepts for Fire Retardancy*, American Chemical Society; ACS Publications: Washington, DC, USA, 2009; ISBN 13-9780841269880.
14. Kinetics Neo Software, Product Version 2.6.6.7, Build Date: 11/16/2022, NETZSCH Company, Germany. 2022. Available online: <https://kinetics.netzscht.com/en> (accessed on 12 February 2022).
15. Janković, B.; Manić, N. Kinetic analysis and reaction mechanism of *p*-alkoxybenzyl alcohol ([4-(hydroxymethyl)phenoxy]methyl)polystyrene) resin pyrolysis: Revealing new information on thermal stability. *Polym. Degrad. Stab.* **2021**, *189*, 109606. [[CrossRef](#)]
16. Faravelli, T.; Pinciroli, M.; Pisano, F.; Bozzano, G.; Dente, M.; Ranzi, E. Thermal degradation of polystyrene. *J. Anal. Appl. Pyrol.* **2001**, *60*, 103–121. [[CrossRef](#)]
17. Gijsman, P. Review on the thermo-oxidative degradation of polymers during processing and in service. *e-Polymers* **2008**, *8*, 727–760. [[CrossRef](#)]
18. Wnorowska, J.; Ciukaj, S.; Kalisz, S. Thermogravimetric analysis of solid biofuels with additive under air atmosphere. *Energies* **2021**, *14*, 2257. [[CrossRef](#)]
19. Dolog, L.; David, K.-H. Zur autoxydation von polystyrol. *Die Makromol. Chem.* **1971**, *145*, 67–84. [[CrossRef](#)]
20. McNeill, I.C.; Razumovskii, L.P.; Gol'dberg, V.M.; Zaikov, G.E. The thermo-oxidative degradation of polystyrene. *Polym. Degrad. Stab.* **1994**, *45*, 47–55. [[CrossRef](#)]
21. Rossi, M.; Camino, G.; Luda, M.P. Characterisation of smoke in expanded polystyrene combustion. *Polym. Degrad. Stab.* **2001**, *74*, 507–512. [[CrossRef](#)]
22. Nazarenko, O.B.; Lipchansky, D.S.; Smirnova, I.N. Effect of iron nanopowder on flammability of epoxy composites. *IOP Conf. Ser. Mater. Sci. Eng.* **2021**, *1019*, 012001. [[CrossRef](#)]
23. Lyon, R.E.; Demario, J. Flammability of glass fiber-reinforced polymer composites. In Proceedings of the 4th International Conference on Composites in Fire, University of Newcastle upon Tyne, Newcastle upon Tyne, UK, 15–16 September 2005.
24. Vyazovkin, S.V.; Goryachko, V.I.; Lesnikovich, A.I. An approach to the solution of the inverse kinetic problem in the case of complex processes. Part III. Parallel independent reactions. *Thermochim. Acta* **1992**, *197*, 41–51. [[CrossRef](#)]
25. Sbirrazzuoli, N.; Vincent, L.; Bouillard, J.; Elégant, L. Isothermal and non-isothermal kinetics when mechanistic information available. *J. Therm. Anal. Calorim.* **1999**, *56*, 783–792. [[CrossRef](#)]
26. Fuentes, C.; Lerner, J.C.; Vázquez, P.; Sambeth, J. Analysis of the emission of PAH in the thermal and catalytic pyrolysis of polystyrene. *Cat. Today* **2021**, *372*, 175–182. [[CrossRef](#)]
27. Chicco, D.; Warrens, M.J.; Jurman, G. The coefficient of determination R-squared is more informative than SMAPE, MAE, MAPE, MSE and RMSE in regression analysis evaluation. *PeerJ Comp. Sci.* **2021**, *7*, e623. [[CrossRef](#)] [[PubMed](#)]
28. Sobek, S.; Werle, S. Kinetic modelling of waste wood devolatilization during pyrolysis based on thermogravimetric data and solar pyrolysis reactor performance. *Fuel* **2020**, *261*, 116459. [[CrossRef](#)]
29. Freund, R.J.; Wilson, W.J. *Statistical Methods*, 2nd ed.; Academic Press: Cambridge, MA, USA; Elsevier Science: San Diego, CA, USA, 2003; pp. 1–668.
30. Levchik, G.F.; Si, K.; Levchik, S.V.; Camino, G.; Wilkie, C.A. The correlation between cross-linking and thermal stability: Cross-linked polystyrenes and polymethacrylates. *Polym. Degrad. Stab.* **1999**, *65*, 395–403. [[CrossRef](#)]
31. Straus, S.; Madorsky, S.L. Thermal stability of polydivinylbenzene and of copolymers of styrene with divinylbenzene and with trivinylbenzene. *J. Res. Natl. Bur. Stand. A Phys. Chem.* **1961**, *65*, 243–248. [[CrossRef](#)] [[PubMed](#)]

32. Li, Z.; Feng, J.; Tian, R.; Lu, C. Multi-step polymer degradation kinetics using activation energy-dependent cataluminescence. *Green Chem.* **2022**, *24*, 2423–2428. [[CrossRef](#)]
33. Huang, J.; Li, X.; Meng, H.; Tong, H.; Cai, X.; Liu, J. Studies on pyrolysis mechanisms of syndiotactic polystyrene using DFT method. *Chem. Phys. Lett.* **2020**, *747*, 137334. [[CrossRef](#)]
34. Jellinek, H.H.G.; Lipovac, S.N. Diffusion-controlled oxidative degradation of isotactic polystyrene at elevated temperatures. II. Kinetics and mechanism. *Macromolecules* **1970**, *3*, 237–242. [[CrossRef](#)]
35. McNeill, I.C. Thermal degradation of polystyrene in different environments. *Die Angew. Makromol. Chem.* **1997**, *247*, 179–195. [[CrossRef](#)]
36. McNeill, I.C.; Zulfiqar, M.; Kousar, T. A detailed investigation of the products of the thermal degradation of polystyrene. *Polym. Degrad. Stab.* **1990**, *28*, 131–151. [[CrossRef](#)]
37. Madras, G.; Smith, J.M.; McCoy, B.J. Degradation of poly(methyl methacrylate) in solution. *Ind. Eng. Chem. Res.* **1996**, *35*, 1795–1800. [[CrossRef](#)]
38. Huang, J.B.; Zeng, G.S.; Li, X.S.; Cheng, X.C.; Tong, H. Theoretical studies on bond dissociation enthalpies for model compounds of typical plastic polymers. *IOP Conf. Ser. Earth Environ. Sci.* **2018**, *167*, 012029. [[CrossRef](#)]
39. Choi, Y.S.; Singh, R.; Zhang, J.; Balasubramanian, G.; Sturgeon, M.R.; Katahira, R.; Chupka, G.; Beckham, G.T.; Shanks, B.H. Pyrolysis reaction networks for lignin model compounds: Unraveling thermal deconstruction of β -O-4 and α -O-4 compounds. *Green Chem.* **2016**, *18*, 1762–1773. [[CrossRef](#)]
40. Challa, P.; Enumula, S.S.; Reddy, S.K.; Kondeboina, M.; Burri, D.R.; Kamaraju, S.R.R. Catalytic conversion of benzyl alcohol to benzaldehyde over a Cu-CeO₂ catalyst: Utilization of CO₂ for enhancement of selectivity and activity. *Ind. Eng. Chem. Res.* **2020**, *59*, 17720–17728. [[CrossRef](#)]
41. Sankar, M.; Nowicka, E.; Carter, E.; Murphy, D.M.; Knight, D.W.; Bethell, D.; Hutchings, G.J. The benzaldehyde oxidation paradox explained by the interception of peroxy radical by benzyl alcohol. *Nature Comm.* **2014**, *5*, 3332. [[CrossRef](#)]
42. Xia, W.; Xu, T.; Wang, H.; Pan, Y. Combustion kinetics of asphalt binder components and the release processes of gaseous products. *Comb. Flame* **2019**, *206*, 322–333. [[CrossRef](#)]
43. Kropotova, S.S.; Kuznetsov, G.V.; Strizhak, P.A. Numerical parametric analysis of the decomposition and propagation of combustion products in a confined environment in the early stages of a fire. *Int. J. Heat Mass Trans.* **2024**, *221*, 125067. [[CrossRef](#)]
44. Sinha, S.; Raj, A. Polycyclic aromatic hydrocarbon (PAH) formation from benzyl radicals: A reaction kinetics study. *Phys. Chem. Chem. Phys.* **2016**, *18*, 8120–8131. [[CrossRef](#)]
45. Parker, D.S.N.; Kaiser, R.I.; Kostko, O.; Ahmed, M. Selective formation of indene through the reaction of benzyl radicals with acetylene. *ChemPhysChem* **2015**, *16*, 2091–2093. [[CrossRef](#)]
46. Sikes, T.; Banyon, C.; Schwind, R.A.; Lynch, P.T.; Comandini, A.; Sivaramakrishnan, R.; Tranter, R.S. Initiation reactions in the high temperature decomposition of styrene. *Phys. Chem. Chem. Phys.* **2021**, *23*, 18432–18448. [[CrossRef](#)] [[PubMed](#)]
47. Howard, J.A.; Ingold, K.U. Absolute rate constants for hydrocarbon autoxidation: III. α -methylstyrene, β -methylstyrene, and indene. *Can. J. Chem.* **1966**, *44*, 1113–1118. [[CrossRef](#)]
48. Jin, H.; Liu, D.; Zou, J.; Hao, J.; Shao, C.; Sarathy, S.M.; Farooq, A. Chemical kinetics of hydroxyl reactions with cyclopentadiene and indene. *Comb. Flame* **2020**, *217*, 48–56. [[CrossRef](#)]
49. Russell, G.A. Oxidation of unsaturated compounds. III. Products of the reaction of indene and oxygen; Stereochemistry of the addition of a peroxy radical and oxygen to a double bond. *J. Am. Chem. Soc.* **1956**, *78*, 1035–1040. [[CrossRef](#)]
50. Pecha, M.B.; Arbelaez, J.I.M.; Garcia-Perez, M.; Chejne, F.; Ciesielski, P.N. Progress in understanding the four dominant intra-particle phenomena of lignocellulose pyrolysis: Chemical reactions, heat transfer, mass transfer, and phase change. *Green Chem.* **2019**, *21*, 2868–2898. [[CrossRef](#)]
51. Pyle, D.L.; Zaror, C.A. Heat transfer and kinetics in the low temperature pyrolysis of solids. *Chem. Eng. Sci.* **1984**, *39*, 147–158. [[CrossRef](#)]
52. Zheng, Z.; Li, Y.; Shi, L.; Chen, D.; Zhang, C.; Wang, J.; Li, P. An experimental and kinetic modeling study on the autoignition characteristics of indene. *Comb. Flame* **2021**, *230*, 111448. [[CrossRef](#)]
53. García-Sánchez, J.T.; Valderrama-Zapata, R.; Acevedo-Córdoba, L.F.; Pérez-Martínez, D.; Rincón-Ortíz, S.; Baldovino-Medrano, V.G. Calculation of mass transfer limitations for a gas-phase reaction in an isothermal fixed bed reactor: Tutorial and sensitivity analysis. *ACS Cat.* **2023**, *13*, 6905–6918. [[CrossRef](#)]
54. Misurya, S.; Morozov, V.; Donskoy, I.; Shlegel, N.; Dorokhov, V. Combustion of liquid fuels in the presence of CO₂ hydrate powder. *Fire* **2023**, *6*, 318. [[CrossRef](#)]
55. Chen, R.; Li, Q.; Xu, X.; Zhang, D.; Hao, R. Combustion characteristics, kinetics and thermodynamics of *Pinus Sylvestris* pine needle via non-isothermal thermogravimetry coupled with model-free and model-fitting methods. *Case Stud. Therm. Eng.* **2020**, *22*, 100756. [[CrossRef](#)]
56. Tang, L.; Xiao, J.; Mao, Q.; Zhang, Z.; Yao, Z.; Zhu, X.; Ye, S.; Zhong, Q. Thermogravimetric analysis of the combustion characteristics and combustion kinetics of coals subjected to different chemical demineralization processes. *ACS Omega* **2022**, *7*, 13998–14008. [[CrossRef](#)] [[PubMed](#)]
57. Diao, R.; Lu, H.; Yang, Y.; Bai, J.; Zhu, X. Comparative insights into flue gas-to-ash characteristics on co-combustion of walnut shell and bio-oil distillation sludge under atmospheric and oxy-fuel condition. *Comb. Flame* **2022**, *246*, 112383. [[CrossRef](#)]

58. Jia, G. Combustion characteristics and kinetic analysis of biomass pellet fuel using thermogravimetric analysis. *Processes* **2021**, *9*, 868. [[CrossRef](#)]
59. Doyle, C. Kinetic analysis of thermogravimetric data. *J. Appl. Polym. Sci.* **1961**, *5*, 285–292. [[CrossRef](#)]
60. Senum, G.I.; Yang, R.T. Rational approximations of the integral of the Arrhenius function. *J. Therm. Anal. Calorim.* **1977**, *11*, 445–447. [[CrossRef](#)]
61. Wanjun, T.; Yuwen, L.; Hen, Z.; Zhiyong, W.; Cunxin, W. New temperature integral approximate formula for non-isothermal kinetic analysis. *J. Therm. Anal. Calorim.* **2003**, *74*, 309–315. [[CrossRef](#)]
62. Pérez-Maqueda, L.A.; Criado, J. The accuracy of Senum and Yang's approximations to the Arrhenius integral. *J. Therm. Anal. Calorim.* **2000**, *60*, 909–915. [[CrossRef](#)]
63. Vyazovkin, S. Evaluation of activation energy of thermally stimulated solid-state reactions under arbitrary variation of temperature. *J. Comput. Chem.* **1997**, *18*, 393–402.
64. Sbirrazzuoli, N. Determination of pre-exponential factor and reaction mechanism in a model-free way. *Thermochim. Acta* **2020**, *691*, 178707. [[CrossRef](#)]
65. Liavitskaya, T.; Vyazovkin, S. All you need to know about the kinetics of thermally stimulated reactions occurring on cooling. *Molecules* **2019**, *24*, 1918. [[CrossRef](#)]
66. Das, P.; Tiwari, P. Thermal degradation kinetics of plastics and model selection. *Thermochim. Acta* **2017**, *654*, 191–202. [[CrossRef](#)]
67. Vyazovkin, S. Determining preexponential factor in model-free kinetic methods: How and why? *Molecules* **2021**, *26*, 3077. [[CrossRef](#)] [[PubMed](#)]
68. Choudhary, J.; Alawa, B.; Chakma, S. Insight into the kinetics and thermodynamic analyses of co-pyrolysis using advanced isoconversional method and thermogravimetric analysis: A multi-model study of optimization for enhanced fuel properties. *Process Saf. Environ. Prot.* **2023**, *173*, 507–528. [[CrossRef](#)]
69. Moukhina, E. Comparison of isothermal predictions based on model-free and model-based kinetic methods. *J. Test. Eval.* **2014**, *42*, 1377–1386. [[CrossRef](#)]
70. Sobek, S.; Werle, S. Solar pyrolysis of waste biomass: Part 2 kinetic modeling and methodology of the determination of the kinetic parameters for solar pyrolysis of sewage sludge. *Renew. Energy* **2020**, *153*, 962–974. [[CrossRef](#)]
71. Roduit, B.; Borgeat, C.; Berger, B.; Folly, P.; Alonso, B.; Aebischer, J.N.; Stoessel, F. Advanced kinetic tools for the evaluation of decomposition reactions—Determination of thermal stability of energetic materials. *J. Therm. Anal. Calorim.* **2005**, *80*, 229–236. [[CrossRef](#)]
72. Ticmanis, U.; Pantel, G.; Wilker, S.; Kaiser, M. Precision required for parameters in thermal safety simulations. In Proceedings of the 32nd International Annual Conference of ICT, Karlsruhe, Germany, 3–6 July 2001; p. 135.
73. Folly, P. Thermal stability of explosives. *Chimia* **2004**, *58*, 394. [[CrossRef](#)]
74. Pastré, J.; Wörsdörfer, U.; Keller, A.; Hungerbühler, K. Comparison of different methods for estimating TMRad from dynamic DSC measurements with ADT 24 values obtained from adiabatic Dewar experiments. *J. Loss Prev. Process Ind.* **2000**, *13*, 7–17. [[CrossRef](#)]
75. Frank-Kamenetskii, D.A. *Diffusion and Heat Transfer in Chemical Kinetics*; Plenum Press: New York, NY, USA; London, UK, 1969; pp. 35–48.
76. Dien, J.M.; Fierz, H.; Stoessel, F.; Killé, G. The thermal risk of autocatalytic decompositions: A kinetic study. *Chimia* **1994**, *48*, 542–550. [[CrossRef](#)]
77. Roduit, B. Advanced Kinetics-Based Simulation Method for Determination of the Thermal Aging, Thermal Runaway TMRad and SADT Using DSC, Analysis Report (Example). The AKTS AG Advanced Kinetics and Technology Solutions. pp. 22–29. Available online: <http://www.akts.com> (accessed on 11 June 2008).
78. Kossoy, A.; Misharev, P.; Belochvostov, V. Peculiarities of Calorimetric Data Processing for Kinetics Evaluation in Reaction Hazard Assessment. In Proceedings of the Conference: 53rd Annual Calorimetry Conference, Midland, MI, USA, 9–14 August 1998; pp. 1–9.
79. Fisher, H.G.; Forrest, H.S.; Grossel, S.S.; Huff, J.E.; Muller, A.R.; Noronha, J.A.; Shaw, D.A.; Tilley, B.J. *Emergency Relief System Design Using DIERS Technology: The Design Institute for Emergency Relief Systems (DIERS) Project Manual*; John Wiley & Sons, Inc., Publication: New York, NY, USA, 1993; pp. 1–488. ISBN 978-0-816-90568-3.
80. Huff, J.E. Emergency venting requirements. *Plant/Oper. Prog.* **1982**, *1*, 211–229. [[CrossRef](#)]
81. Gygax, R. Chemical reaction engineering for safety. *Chem. Eng. Sci.* **1988**, *43*, 1759–1771. [[CrossRef](#)]

Disclaimer/Publisher's Note: The statements, opinions and data contained in all publications are solely those of the individual author(s) and contributor(s) and not of MDPI and/or the editor(s). MDPI and/or the editor(s) disclaim responsibility for any injury to people or property resulting from any ideas, methods, instructions or products referred to in the content.